

REPORT DOCUMENTATION PAGE

Form Approved OMB NO. 0704-0188

The public reporting burden for this collection of information is estimated to average 1 hour per response, including the time for reviewing instructions, searching existing data sources, gathering and maintaining the data needed, and completing and reviewing the collection of information. Send comments regarding this burden estimate or any other aspect of this collection of information, including suggestions for reducing this burden, to Washington Headquarters Services, Directorate for Information Operations and Reports, 1215 Jefferson Davis Highway, Suite 1204, Arlington VA, 22202-4302. Respondents should be aware that notwithstanding any other provision of law, no person shall be subject to any penalty for failing to comply with a collection of information if it does not display a currently valid OMB control number.  
PLEASE DO NOT RETURN YOUR FORM TO THE ABOVE ADDRESS.

1. REPORT DATE (DD-MM-YYYY) 08-05-2009		2. REPORT TYPE Final Report		3. DATES COVERED (From - To) 1-Jun-2004 - 31-May-2008	
4. TITLE AND SUBTITLE Understanding the Plasma-Propellant Interaction through Experimental Modeling			5a. CONTRACT NUMBER W911NF-04-1-0213		
			5b. GRANT NUMBER		
6. AUTHORS Rik Blumenthal			5c. PROGRAM ELEMENT NUMBER 611102		
			5d. PROJECT NUMBER 611102		
			5e. TASK NUMBER		
			5f. WORK UNIT NUMBER		
7. PERFORMING ORGANIZATION NAMES AND ADDRESSES Auburn University Office of Sponsored Programs Auburn University Auburn University, AL 36849 -5131				8. PERFORMING ORGANIZATION REPORT NUMBER	
9. SPONSORING/MONITORING AGENCY NAME(S) AND ADDRESS(ES) U.S. Army Research Office P.O. Box 12211 Research Triangle Park, NC 27709-2211				10. SPONSOR/MONITOR'S ACRONYM(S) ARO	
				11. SPONSOR/MONITOR'S REPORT NUMBER(S) 43064-CH.8	
12. DISTRIBUTION AVAILABILITY STATEMENT Approved for public release; Distribution Unlimited					
13. SUPPLEMENTARY NOTES The views, opinions and/or findings contained in this report are those of the author(s) and should not be construed as an official Department of the Army position, policy or decision, unless so designated by other documentation.					
14. ABSTRACT The goal of the project was to develop an understanding of the plasma-propellant interaction, specifically the ignition of RDX by ETC. Based on experimental modeling results a model of ETC ignition was developed in which ignition occurs through a process that resembles that of a primary explosive more than a secondary explosive. In this process, hydrogen ions in the ETC igniter plasma implant into the RDX surface and are rapidly neutralized. The resulting hydrogen atoms then attack an RDX molecule, abstracting a hydrogen atom from one of					
15. SUBJECT TERMS RDX, Propellant, Ignition, Laser Ablation, Plasma					
16. SECURITY CLASSIFICATION OF:			17. LIMITATION OF ABSTRACT SAR	15. NUMBER OF PAGES	19a. NAME OF RESPONSIBLE PERSON Rik Blumenthal
a. REPORT U	b. ABSTRACT U	c. THIS PAGE U			19b. TELEPHONE NUMBER 334-844-6963

## Report Title

### Understanding the Plasma-Propellant Interaction through Experimental Modeling

#### ABSTRACT

The goal of the project was to develop an understanding of the plasma-propellant interaction, specifically the ignition of RDX by ETC. Based on experimental modeling results a model of ETC ignition was developed in which ignition occurs through a process that resembles that of a primary explosive more than a secondary explosive. In this process, hydrogen ions in the ETC igniter plasma implant into the RDX surface and are rapidly neutralized. The resulting hydrogen atoms then attack an RDX molecule, abstracting a hydrogen atom from one of the CH<sub>2</sub> groups to form a sub-surface hydrogen molecule. Loss of hydrogen triggers double bond formation releasing a NO<sub>2</sub> molecule. Confined to the same volume of space, the NO<sub>2</sub> and H<sub>2</sub> rapidly react to form NO and H<sub>2</sub>O releasing heat directly at the site of reaction. Heat release directly at the reaction site is characteristic of a primary explosive and results in rapid thermal run-away and ultimately in ignition. In addition to this work, a new ignition method has been developed that uses the laser ablation of a polymer overlayer to form a plasma that ignites the RDX. Finally, investigations of this new ignition method have led to fundamental studies of laser ablation.

---

#### List of papers submitted or published that acknowledge ARO support during this reporting period. List the papers, including journal references, in the following categories:

##### (a) Papers published in peer-reviewed journals (N/A for none)

T.A. Bormotova and R. Blumenthal, "Ultraviolet (UV) Laser Ablation of Polycarbonate and Glass in Air," Journal of Applied Physics, 105(3) (2009) 034910/1-034910/7.

Rodney Valliere and Rik Blumenthal, "Strong Synergistic Effects in the Combustion of Propellants in H<sub>2</sub> Plasmas," Journal of Applied Physics, 100(8) (2006) 084904/1-084904/7.

Aaron S. Orland and Rik Blumenthal, "A nebulizing spray technique for the deposition of propellant thin films," Journal of Propulsion and Power 21(3) (2005) 571-573.

Rik Blumenthal and Sharon F. Webb, "Role of Neutral Molecule Chemistry In Electron Cyclotron Resonance Microwave Plasmas Capable of Diamond Deposition," Journal of Vacuum Science and Technology B, 24(2) (2006) 643-650.

Aaron S. Orland and Rik Blumenthal, "Metal Etching with Organic Based Plasmas: II. CO/NH<sub>3</sub> Plasmas" Journal of Vacuum Science and Technology B 23(4) (2005) 1597-1602.

Aaron S. Orland and Rik Blumenthal, "Magnetic Metal Etching with Organic Based Plasmas: I. CO/H<sub>2</sub> Plasmas" Journal of Vacuum Science and Technology B 23(4) (2005) 1589-1596.

**Number of Papers published in peer-reviewed journals:** 6.00

---

##### (b) Papers published in non-peer-reviewed journals or in conference proceedings (N/A for none)

**Number of Papers published in non peer-reviewed journals:** 0.00

---

##### (c) Presentations

“Small (<1g) Scale Materials Characterization for Screening New Energetic Materials” JANNAF Workshop on R&D Required to Implement New Energetic Ingredients in Munitions, Aberdeen MD, August 29-31, 2006.

“Investigating the Interaction of High Pressure, High Temperature Plasmas with Propellant Surfaces through Experimental Modeling” American Vacuum Society, 51st International Symposium, Boston MA, Contributed Talk, November 4, 2005

“Investigating the Plasma Propellant Interaction through Experimental Modeling” American Vacuum Society, 52st International Symposium, Boston MA, Contributed Talk, November 3, 2005.

“Extending the ‘Winters and Coburn Method’ to Plasma Propellant Interactions” American Vacuum Society, 51st International Symposium, Anaheim CA, Contributed Poster, November 16, 2004.

“Chemistry in Plasmas” Jacksonville State University, Invited Talk (Graduate Recruitment), January 28, 2004

“Model Studies of the Plasma Propellant Interaction” ARO Workshop on PPI, Aberdeen MD, Invited Talk, October 30, 2003

“Plasma Interactions with RDX” U.S Army Research Laboratory, Aberdeen MD, Invited Talk, August 8, 2003

**Number of Presentations:** 7.00

---

**Non Peer-Reviewed Conference Proceeding publications (other than abstracts):**

**Number of Non Peer-Reviewed Conference Proceeding publications (other than abstracts):** 0

---

**Peer-Reviewed Conference Proceeding publications (other than abstracts):**

**Number of Peer-Reviewed Conference Proceeding publications (other than abstracts):** 0

---

**(d) Manuscripts**

**Number of Manuscripts:** 0.00

---

**Number of Inventions:**

---

**Graduate Students**

<u>NAME</u>	<u>PERCENT SUPPORTED</u>
Atrem Dyachenko	0.50
Huijiao Sun	0.50
Rodney Valliere	1.00
<b>FTE Equivalent:</b>	<b>2.00</b>
<b>Total Number:</b>	<b>3</b>

---

**Names of Post Doctorates**

<u>NAME</u>	<u>PERCENT SUPPORTED</u>
Tatiana Bormotova	1.00
<b>FTE Equivalent:</b>	<b>1.00</b>
<b>Total Number:</b>	<b>1</b>

---

**Names of Faculty Supported**

<u>NAME</u>	<u>PERCENT SUPPORTED</u>	National Academy Member
Rik Blumenthal	0.08	No
<b>FTE Equivalent:</b>	<b>0.08</b>	
<b>Total Number:</b>	<b>1</b>	

**Names of Under Graduate students supported**

<u>NAME</u>	<u>PERCENT SUPPORTED</u>
Dustin Kosar	1.00
Michael Hunt	1.00
<b>FTE Equivalent:</b>	<b>2.00</b>
<b>Total Number:</b>	<b>2</b>

**Student Metrics**

This section only applies to graduating undergraduates supported by this agreement in this reporting period

- The number of undergraduates funded by this agreement who graduated during this period: ..... 1.00
- The number of undergraduates funded by this agreement who graduated during this period with a degree in science, mathematics, engineering, or technology fields:..... 1.00
- The number of undergraduates funded by your agreement who graduated during this period and will continue to pursue a graduate or Ph.D. degree in science, mathematics, engineering, or technology fields:..... 0.00
- Number of graduating undergraduates who achieved a 3.5 GPA to 4.0 (4.0 max scale):..... 0.00
- Number of graduating undergraduates funded by a DoD funded Center of Excellence grant for Education, Research and Engineering:..... 0.00
- The number of undergraduates funded by your agreement who graduated during this period and intend to work for the Department of Defense ..... 1.00
- The number of undergraduates funded by your agreement who graduated during this period and will receive scholarships or fellowships for further studies in science, mathematics, engineering or technology fields: ..... 0.00

**Names of Personnel receiving masters degrees**

<u>NAME</u>
Artem Dyachenko
<b>Total Number:</b>
<b>1</b>

**Names of personnel receiving PHDs**

<u>NAME</u>
<b>Total Number:</b>

**Names of other research staff**

<u>NAME</u>	<u>PERCENT SUPPORTED</u>
<b>FTE Equivalent:</b>	
<b>Total Number:</b>	

**Sub Contractors (DD882)**

**Inventions (DD882)**

# Final Technical Report

## Understanding the Plasma-Propellant Interaction through Experimental Modeling W911NF-04-1-0213, Rik Blumenthal, Principal Investigator

Table of Contents .....	i
Table of Figures .....	ii
I. Goals of Project and Summary of Results .....	1
II. Investigation of the Mechanism of ETC Ignition .....	1
A. Experimental Modeling – Background and Application to ETC Ignition .....	1
B. Thin Film Spray Deposition Method .....	3
C. Erosion of RDX films in Hydrogen and Argon Plasmas .....	4
D. Erosion of RDX films under Energetic Electron and Photon Irradiation .....	7
E. Model of the Ignition Process .....	8
F. A New Understanding of RDX Insensitivity, Ignition, Combustion and Detonation	10
III. Laser Ignition of RDX Using Polymer Overlayers.....	11
A. Gas Pressure Jump Studies .....	12
B. Photographic Image Studies .....	13
C. Outlook for Future Progress in Photographic Imaging.....	16
IV. Fundamental Studies of Laser Ablation.....	16
A. Dynamic Pressure Measurements During Laser Ablation.....	16
B. Laser Ablation of Polycarbonate and Glass.....	19
C. Photodeflection Studies of the Laser Ablation of RDX .....	22
D. Outlook for Future Progress in Photodeflection Studies .....	22
V. Summary and Conclusions .....	29
Bibliography .....	30

## List of Figures

Figure 1 - Silicon etch rate measured under exposure to different substitutes for the components of an F <sub>2</sub> plasma, from reference 1. ....	2
Figure 2 - Output of an ETC igniter from Nusca et al. from reference 2.....	2
Figure 3 - The nebulizing spray deposition apparatus. The N <sub>2</sub> sheath gas is introduced at the bottom while the RDX solution is introduced through the capillary at the top.....	3
Figure 4 - Discontinuous film used for erosion studies showing 10 μm crystallites and machining grooves of sample holder.....	3
Figure 5 - RDX spot with 1mm hole laser ablated through it. ....	4
Figure 6 - Basic experimental setup: the ECR-microwave plasma functioned as the source of ions, electrons and chemically reactive species, while the diode laser illuminated the film for video recording. ....	4
Figure 7 - First-order plot of the erosion of an RDX film in an argon plasma under various plasma conditions. ....	5
Figure 8 - A plot of the first-order rate constants for the erosion of RDX in argon plasmas as function of applied bias (solid line) and the best fit for the theoretical sputter yield (dashed line).....	5
Figure 9 - Erosion of RDX films in H <sub>2</sub> and Ar Plasmas. ....	6
Figure 10 - Plot of the erosion of an RDX film in a hydrogen plasma under different applied positive biases. ....	7
Figure 11- Erosion of RDX with and without a quartz window placed above the film. ....	8
Figure 12- The proposed mechanism of hydrogen atoms implanted in RDX. ....	9
Figure 13- Pressure trace of the ablation of bare RDX.....	12
Figure 14- Pressure trace of the ablation of polycarbonate coated RDX.....	13
Figure 15- Fireball created by the ablation of polycarbonate in air.....	13
Figure 16- Successive video images obtained during the ablation of bare RDX.....	14
Figure 17- Video images obtained during the ablation of polycarbonate coated RDX.....	15
Figure 18- Experimental apparatus used in dynamic pressure measurement and photodeflection experiments. ....	16
Figure 19- Sandwich structure used to reduce mass addition to the pressure gauge.....	17
Figure 20 - Dynamic pressure measurements of sandwich structures of polycarbonate/RDX/polycarbonate (left) and polycarbonate/RDX/parafilm (right).....	18

Figure 21-	Photodeflection curves for the ablation of polycarbonate as a function of surface to probe distance .....	20
Figure 22-	Photodeflection curves for the ablation of glass as a function of surface to probe distance .....	21
Figure 23-	Normalized photodeflection data for the first laser shot on an RDX film. ....	23
Figure 24-	Normalized photodeflection data for the second laser shot on an RDX film. ....	24
Figure 25-	Normalized photodeflection data for the third laser shot on an RDX film. ....	25
Figure 26-	Normalized photodeflection data for the fourth laser shot on an RDX film .....	26
Figure 27-	Normalized photodeflection data for the fifth laser shot on an RDX film. ....	27
Figure 28 -	Normalized photodeflection data for the sixth laser shot on an RDX film. ....	28

## I. Goals of Project and Summary of Results

The overall goal of the project was, as the proposal title indicated, to develop an understanding of the plasma-propellant interaction, specifically the ignition of RDX by an electrothermal-chemical (ETC) igniter. In terms of that principle goal, the project was a complete success. Based on experimental modeling results that indicated that a) RDX remains unaffected under exposure to electrons, b) is slowly eroded by exposure to generic ions, c) is rapidly eroded when exposed to unbiased hydrogen plasmas, and d) is even more rapidly eroded when exposed to energetic hydrogen ions, a model of ETC ignition was developed in which ignition is achieved through a process that better resembles a primary explosive than a secondary explosive.

The process begins when hydrogen ions in the ETC igniter plasma are implanted into the RDX surface by the self-bias of the plasma. Once implanted, the hydrogen ions are rapidly neutralized. The newly formed hydrogen atoms then attack RDX molecule by abstracting a hydrogen atom from one of the CH<sub>2</sub> groups of the RDX molecule to form a sub-surface hydrogen molecule. Upon loss of the hydrogen atom, the CH group forms a double bond with a neighboring nitrogen atom releasing a NO<sub>2</sub> molecule. Formed in close proximity and confined to the same volume of space by the solid surrounding them, the NO<sub>2</sub> and H<sub>2</sub> will rapidly react to form NO and H<sub>2</sub>O releasing significant heat (54.4 kcal/mol) directly at the site of reaction. Heat release directly at the reactions site is a characteristic of a primary explosive, which results in thermal run-away and ultimately ignition. In traditional ignition of RDX, the initial reaction at the solid surface is endothermic and must be sustained by radiative heating from the reactions in the exothermic reactions in the flame, several millimeters above the surface.

In addition to addressing the principle question of the mechanism of ETC ignition, a new method of ignition has been developed based on the same ignition mechanism but which does not require the large capacitor and power supply that currently make ETC ignition impractical. This new method uses laser ablation of a thin polymer overlayer to initiate the formation of an atomic plasma that then ignites the RDX. Finally, while searching for additional ways to investigate this new laser ignition method, laser ablation of polycarbonate, borosilicate glass and RDX have been investigated using an optical deflection technique. In that work, deflections of the optical probe beam were observed that correlated well with the predictions of gas dynamics

## II. Investigation of the Mechanism of ETC Ignition

### II.A. Experimental Modeling – Background and Application to ETC Ignition

Experimental modeling is an alternative to the direct investigation of complex chemical and physical environments. In this approach, a complex environment is understood through a number of well-defined experiments designed to probe the interactions between combinations of the components of the complex environments. Experimental modeling has been applied previously to understanding the plasma etching of silicon with fluorine.<sup>1</sup> In these experiments, a silicon surface was exposed to XeF<sub>2</sub> gas and Ar<sup>+</sup> ions as substitutes for the fluorine atoms and the fluorine ions found in the plasma, see figure 1. Upon adsorption, XeF<sub>2</sub> gas dissociated into F atoms which reacted with the surface to produce volatile SiF<sub>4</sub> resulting in etching of the silicon. Turning on the Ar<sup>+</sup> ion beam, the rate of etching rose from ~6 Å/minute to a steady state rate of ~57 Å/minute. Upon cessation of the the XeF<sub>2</sub> gas flow, the etching dropped to ~4 Å/minute, corresponding to the sputter rate of silicon under 400 eV Ar<sup>+</sup> ion bombardment. From this result

alone, it can be concluded that a synergy between fluorine atoms and ion bombardment, and neither component by itself, is responsible for the high etch rate observed in the plasma. From this and related data, a current model of plasma etching was developed. In this model, ion bombardment thins the partially reacted  $\text{SiF}_x$  layer on the surface that builds on the surface under fluorine atom exposure. With a thinner reacted layer, fluorine atoms diffuse more easily to the underlying pristine silicon, allowing the etch reaction front to advance exponentially faster into the bulk material.

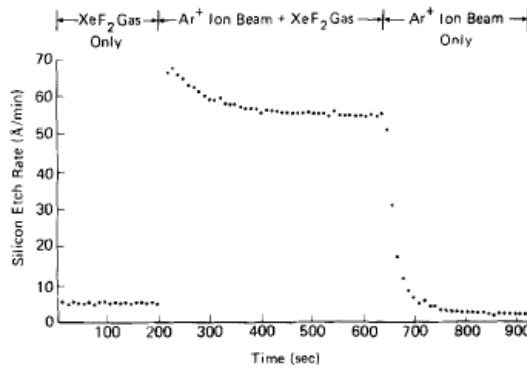


Figure 1 – Silicon etch rate measured under exposure to different substitutes for the components of an  $\text{F}_2$  plasma, from reference 1.

In ETC ignition, a secondary explosive is ignited by exposure to the atomic plasma formed by the capacitive ablation of a polymer tube. The atomic plasma formed in an ETC igniter has been investigated by Nusca et al.<sup>2</sup> The results of their simulations of the chemical composition of the igniter output are shown in figure 2. Immediately after electrical discharge,

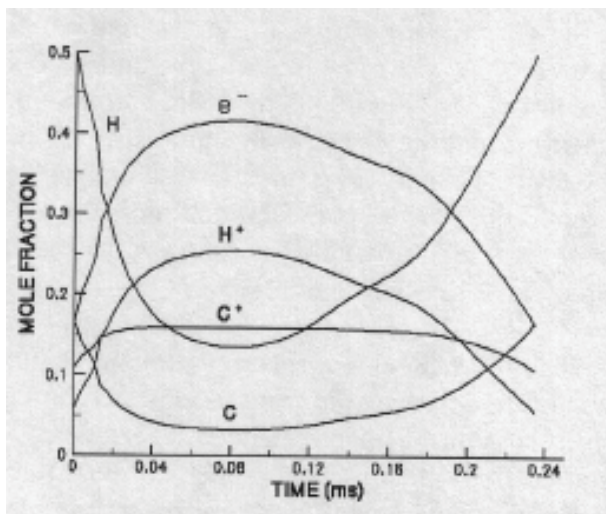


Figure 2 – Output of an ETC igniter from Nusca et al. from reference 2

the output is primarily hydrogen and carbon atoms. After  $\sim 20$  microseconds, the concentrations of electrons and ions rise. The concentrations of electrons and ions peak at  $\sim 100$  microseconds and then fall while the neutral atom concentrations rise. From the perspective of experimental modeling, the Nusca model of the ETC plasma indicates that the species of interest are hydrogen ions and atoms, carbon ions and atoms, and electrons. In addition, the possible role of the ultraviolet (UV) emission of the 30,000K plasma must be considered.

The final element necessary for experimental modeling is a suitable substitute for the propellant grains used in

artillery. In the current work, thin ( $\sim 15\text{-}20 \mu\text{m}$  thick) RDX films were used for this purpose. The films were prepared using a nebulizing spray technique described in detail in section II.B. To investigate the interaction of these films with the various species of interest, the films were prepared on stainless steel sample holders that could be readily transferred into the vacuum chamber that housed an ASTeX model 4300 compact electron cyclotron resonance (ECR) plasma source and the gas nozzle for the supersonic pulse, plasma sampling mass spectrometry, described in detail previously.<sup>3</sup> Using hydrogen as the feed gas, the ECR plasma becomes a source of hydrogen atoms, hydrogen ions, electrons and ultraviolet radiation.

With the RDX film mounted directly below the plasma source, the energies and relative fluxes of the various species impinging on the RDX film can be controlled by adjusting the dc-bias on the sample holder. Under negative sample bias, positive ions such as  $H^+$ ,  $H_2^+$  and  $Ar^+$  can be drawn to the RDX surface with average energies equal to the sum of the applied bias and the  $\sim+15V$  self-bias of the plasma. Under positive sample bias, electrons from the plasma are drawn to the RDX surface. Under zero applied bias, charged species are not drawn to the surface and the effects of the neutral atom flux will be predominant. By placing a window a few millimeters above the RDX film, it is possible to eliminate the flux of charged species and reduce the neutral radical flux, allowing observation of the effect of the UV radiation absent most of the other species. The results of these experiments will be included in section II.C.

## II.B. Thin Film Spray Deposition Method

Two thin film deposition techniques have been developed based on a nebulizing spray technique. The details of the spray technique used to prepare discontinuous ring films of RDX for the erosion studies presented in section II.C has been previously published in the Journal of Propulsion and Power in 2005<sup>4</sup> and a modification of that method which provides continuous films that are tens of micrometers thick for the laser studies has been previously published in Artem Dyachenko's Thesis.<sup>5</sup>

Briefly, a solution of 1.0 mg RDX per milliliter of acetonitrile was purchased from a manufacturer of analytical standards (Cerrillant Corp.) or a 1.0 mg RDX per milliliter of acetonitrile was prepared by dissolution of RDX obtained from Redstone Arsenal. The apparatus is shown in figure 3. The solution is driven through a 32 gauge capillary (0.009-in. O.D. , 0.004-in. I.D.) using a syringe and a syringe pump. The opening of the syringe is placed at the center of a 1/8-in. tube through which dry  $N_2$  is allowed to flow from an input pressure of  $\sim 40$  psi. Upon emerging from the capillary, the solution is torn into droplets by the rapidly flowing of  $N_2$  sheath gas

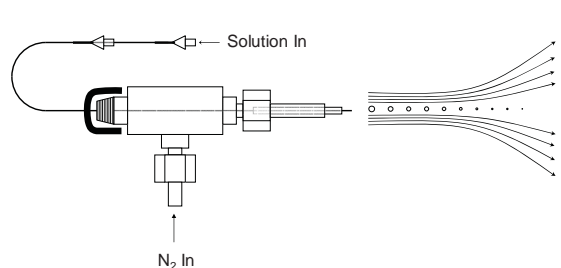


Figure 3 – The nebulizing spray deposition apparatus. The  $N_2$  sheath gas is introduced at the bottom while the RDX solution is introduced through the capillary at the top.

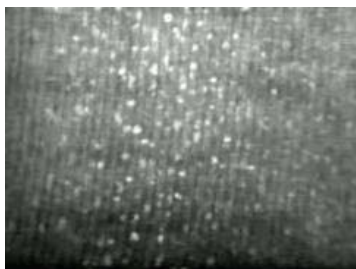


Figure 4 - Discontinuous film used for erosion studies showing  $10\ \mu m$  crystallites and machining grooves of sample holder

surrounding the opening. The droplets are then carried in the gas flow to the substrate on which the RDX is to be deposited. The substrates used where a metal sample holder that was rotated during deposition to produce the discontinuous rings used for the erosion studies, see figure 4, and glass slides or a polycarbonate films that were held stationary during deposition to produce the thin film spots used in the laser studies, see figure 5. During transit, solvent evaporates from the droplets into the dry nitrogen carrier gas. An

approximately 1.5 inch distance between the sprayer and the substrate has proved optimal in allowing solution droplets to become sufficiently desiccated such that uniform films are produced. At closer distances, evidence of dissolution in excess solvent and either re-crystallization at the edges of the liquid deposit at the sample center or transport of RDX crystals from the sample center has been observed. At greater distances, RDX crystallites formed in the gas flow become over desiccated and become too dry to readily stick to the substrate. A 1.0 mm laser ablated hole in the RDX spot was generated to help visualization of the film.

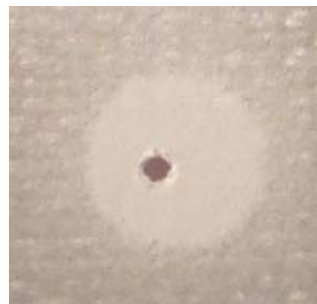


Figure 5 – RDX spot with 1mm hole laser ablated through it.

### II.C. Erosion of RDX films in Hydrogen and Argon Plasmas

Many of the results presented in this section have been previously published in the Journal of Applied Physics in 2006.<sup>3</sup>

The erosion of RDX films by exposure to an ECR-Microwave plasma generated 10'' above the film and magnetically confined to a cylindrical shape was monitored by video recording the glancing incident laser light scattered into a video camera placed 30° from the sample normal, see figure 6. Each video record of film exposure to a plasma was recorded for two hours long or until the entire RDX film had been eroded from the stainless steel sample holder. The video recording was accomplished using a commercial surveillance camera with the infrared illumination LEDs removed connected to a commercial video tape deck. Post-recording, the analog video record was transferred to a computer for digital analysis using a Hauppauge WinTV-USB. The first step in the analysis of the video was to identify of the diameters and thicknesses of individual rings of RDX crystals in the first video frame. Once identified, the pixels corresponding to laser scattering from each ring were summed frame by frame to produce a scattered light intensity (signal) versus time. Analysis of the resulting intensity data was carried out assuming first order kinetics based on the simplifying assumption that the intensity of the scattered light was proportional to the amount of RDX remaining on the surface. The best test of the assumption of first order kinetics was the observation of extended linear regions in plots of the natural logarithm of the scattered light intensity versus time.

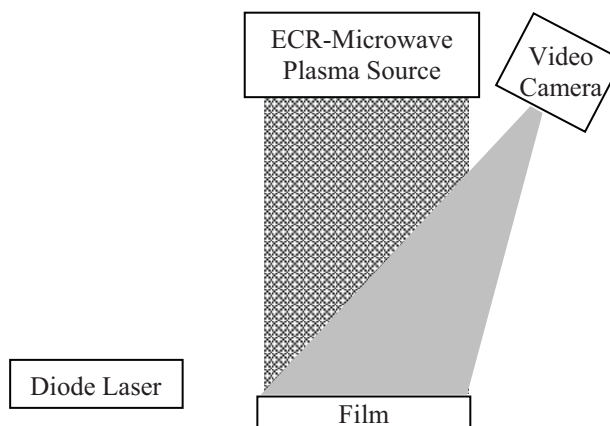


Figure 6 – Basic experimental setup: the ECR-microwave plasma functioned as the source of ions, electrons and chemically reactive species, while the diode laser illuminated the film for video recording.

Erosion of RDX films in plasmas can take place by a number of mechanisms. The first and simplest of these mechanisms is physical erosion or sputtering of the film. Physical sputtering is the ejection of atoms or molecules from a solid as a result of the momentum carried to the surface by energetic ions. Sputtering will always occur when a surface is exposed to a plasma with a potential that is more positive than the solid. In practice, the potential of the solid is far easier to control than the potential of the plasma, so ion bombardment conditions are typically controlled by application of an external (negative) bias on the solid. An important characteristic of physical erosion is that the rate of erosion will increase rapidly with ion energy (negative applied bias) up to a maximum at  $\sim 10\text{kV}$ . The second possible mechanism of erosion is chemical erosion. Chemical erosion occurs when a chemically reactive species impacting on a surface reacts with it to form a volatile product in a net reaction that removes material from the surface. An important characteristic of chemical erosion is that the rate of erosion should, to the first order analysis at least, be independent of the bias. If the chemical erosion rate were to show bias dependence, it would be expected to decrease with increasing ion energy as the time for reaction of reactive ions at the surface decreases. The final mechanism involves a combination of physical and chemical erosion, such that found by Winter and Coburn in the etching of silicon. They found that the rate limiting step for the advancement of the reaction front was the diffusion of reactive species through a partially reacted layer, with ion bombardment, or physical erosion, plays a key role by thinning the reacted layer, exponentially increasing the rate of diffusion through the layer, and dramatically increasing the rate of etching.

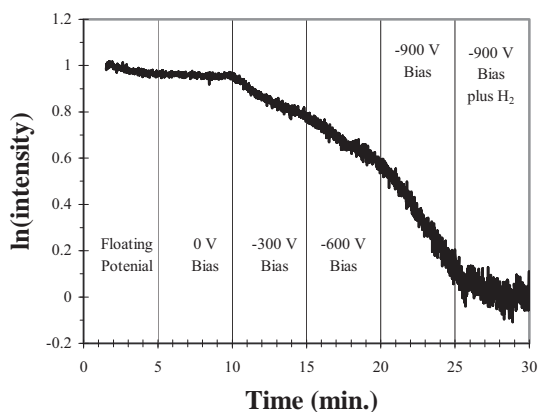


Figure 7 – First-order plot of the erosion of an RDX film in an argon plasma under various plasma conditions.

The Argon is a noble gas, and, hence it does not readily react with the RDX or its decomposition or combustion products. Consequently, the erosion of RDX films in argon plasmas can only proceed by physical erosion. Figure 7 is a plot of the natural logarithm of the scattered light intensity observed as a function of time as an RDX film was exposed to an argon plasma under different sample biases.

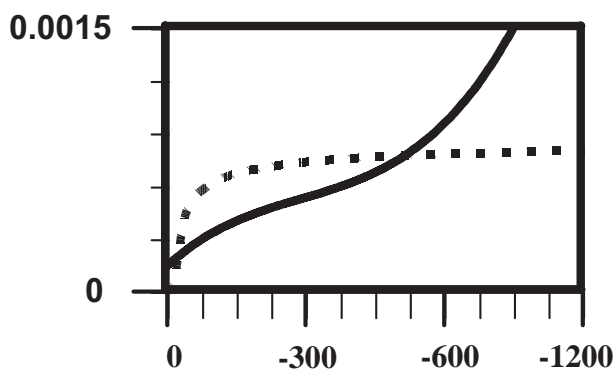


Figure 8 – A plot of the first-order rate constants for the erosion of RDX in argon plasmas as function of applied bias (solid line) and the best fit for the theoretical sputter yield (dashed line).

The first important conclusion that can be clearly drawn from the data in figure 7 is that physical erosion under each bias condition conforms to first-order kinetics, i.e. the data are linear in each region of constant bias. The second important conclusion is that the rate of erosion increases with increasing ion energy as expected for sputtering. Having established that the erosion rate follows first-order kinetics, the first-order rate

constant for physical erosion can be obtained as the negative of the slope of the erosion curve in each linear region. Figure 8 is a plot of the first-order rate constants obtained from the argon plasma data. The solid line is a smooth curve through the data, and the dashed line is a best fit of the data to the mathematical form expected for a traditional Sigmund sputter yield.<sup>6</sup> The figure clearly shows that the erosion of RDX under an argon ion flux process is not consistent with the traditional mechanism observed for the sputtering of normal materials like metals, semiconductors or insulators. Consequently, it may be concluded that chemical processes are initiated by the impact of inert ions on RDX.

When considering the impact of a ion on the surface of any material, significant bond breaking will occur.<sup>7</sup> If the material is an energetic material, it is reasonable to imagine that the bond breaking might result in the formation of reactive species, that once formed, would attack additional molecules, resulting in the removal of significantly more material than would be expected from the physical process of sputtering alone. From another perspective, the ion may be viewed as the source of an impulse of energy and momentum to the surface. The “local pressure” that would be result from the lost half of the momentum of a 400 eV argon in the surface layer assuming a 1nm<sup>2</sup> area would be in excess of 2 x 10<sup>6</sup> atm. The compression resulting from this local pressure would produce a combination of local pressure and temperature well above those required for spontaneous combustion of RDX. However, it is important to note that these local pressure and temperatures would be very short lived, decaying below the threshold fo spontaneous combustion in the first few nanoseconds after impact, resulting in the rapid extinction of the combustion event. Under this model, the amount of material removed by ion impact would be greater than the three or four atoms expected from physical sputtering alone. From either perspective the outcome is the same: the chemical nature of RDX leads to an enhanced removal of material when it is struck by energetic ions.

When an RDX film is exposed to a hydrogen plasma, chemical erosion becomes a possibility. The erosion of an RDX films exposed hydrogen and argon plasmas are shown in figure 9. The most noticeable difference in the erosion of RDX in the two different plasmas is

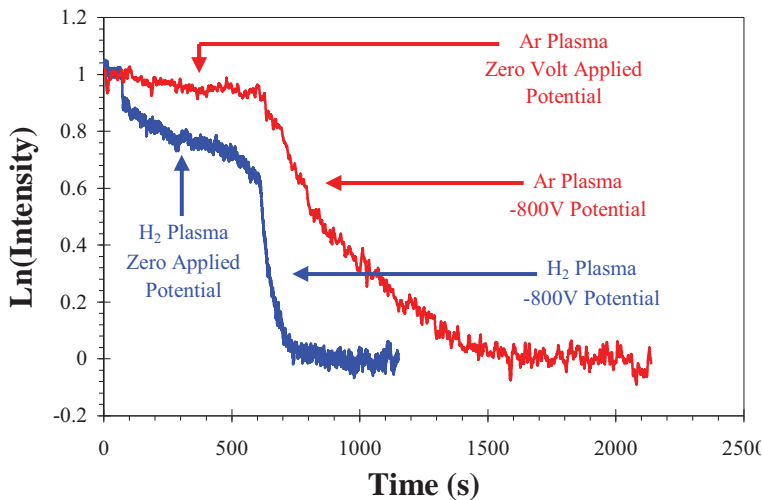


Figure 9 – Erosion of RDX films in H<sub>2</sub> and Ar Plasmas.

the fact that RDX erodes much faster in the hydrogen plasma under both applied biases. The enhanced rate of erosion under zero applied bias (actually ~-15 V relative to the self-bias of the plasma) is a clear indication of chemical erosion. The enhanced rate under large negative bias is more difficult to understand. Physical erosion, or sputtering, simply cannot explain the higher erosion rate in the hydrogen plasma. The low mass of the hydrogen ions in the plasma simply rules out the possibility

that sputtering could be responsible for the observed increase in the erosion rate under large negative bias. Hence, a model of the interaction of the plasma with the RDX is required in which a primarily chemical erosion process at zero applied bias can be octupled with high negative ions bias, i.e. energetic ion bombardment.

#### II.D. Erosion of RDX films under Energetic Electron and Photon Irradiation

Many of the results presented in this section have been previously published in the Journal of Applied Physics in 2006.<sup>3</sup>

Exposure to plasmas under positive sample bias attracts and accelerates electrons to the surface. In argon plasmas at positive bias, the surface is exposure to only to energetic electrons and unreactive, neutral argon atoms. Under

exposure to a applied bias of +100V, no erosion was observed over periods as long as two full hours. To insure that the RDX film had not been modified by exposure to the electron bombardment, hydrogen was introduced to the plasma at the end of each experiment and the applied bias was set to -900V, after which the

RDX film was observed to have been removed in the same few minutes as a virgin film. Under positively bias in hydrogen plasmas, the RDX surface is exposed to both energetic electrons and reactive, neutral hydrogen atoms. Figure 10 is a plot of the natural logarithm of the scattered light intensity as an RDX surface was exposed to different positive biases. Comparing the slopes of the periods of zero bias to those with +25V applied bias reveals a slightly lower slope, or erosion rate, when the more positive bias is applied. At +50V applied bias, the slope once becomes equal to the one observed at zero applied bias. At a biases of +100 and +150 volts applied bias, a slope double that observed at zero applied is observed. Beyond that time, the signal plateaus indicating complete removal of the film. Considering the slope of +25V applied bias to be the rate of erosion due to , the slightly higher erosion rate at zero applied bias can be explained as the result of ion bombardment due to the +15V self bias of the plasma. It was not possible to probe much beyond +150 volts as significant surface charging resulting in bright flashes that temporarily blinded the camera.

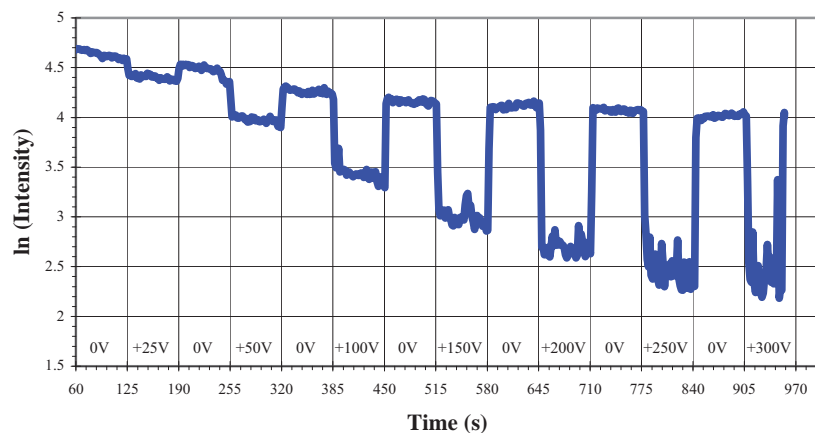


Figure 10 – Plot of the erosion of an RDX film in a hydrogen plasma under different applied positive biases.

The modest increase of the erosion rate at biases more positive than +25V indicates that electron impact does enhance the erosion rate at least in the presence of hydrogen atoms. However, this result is not unexpected as energetic electron impact excitation cross-sections are known to be large. Specifically, electron impact ionization is the most common ionization

method in mass spectrometry due to its high efficiency, maximizing at an electron energy of  $\sim 80$  eV. If 80 eV electrons can efficiently excite electrons in normal molecules to unbound states, it should not be surprising that the same electrons might excite electronic transitions leading to decomposition of energetic materials. It is surprising that the rate of erosion under energetic electron bombardment only becomes significant in the presence of hydrogen, indicating that energetic electron bombardment does not trigger the formation of volatile species, ie. decomposition, but instead triggers only increased reactivity to hydrogen. Overall, the experiments showed that electrons play only a minor role in the erosion of RDX films.

To investigate the erosion of RDX under the influence of the photon flux of the plasma, a quartz window placed  $\sim 2$ mm above an RDX film and the scattered light intensity was recorded

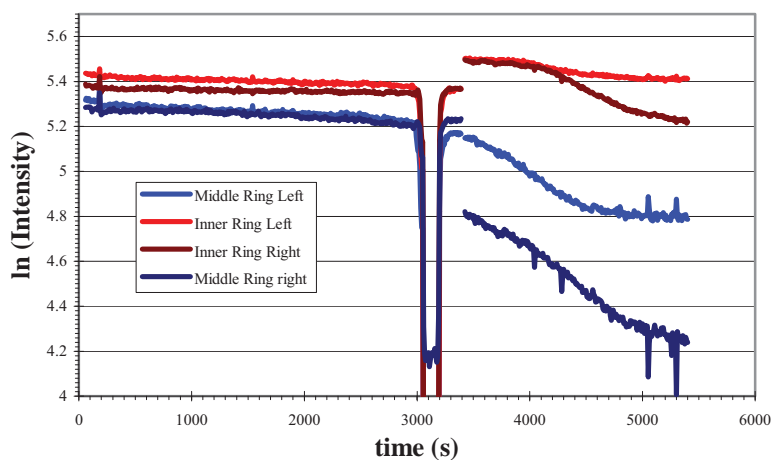


Figure 11 – Erosion of RDX with and without a quartz window placed above the film.

both before and after removal of the window in a hydrogen plasma. Figure 11 is a plot of the natural logarithm of the intensity of light scattered from the portions of the rings of RDX that were clearly visible before and after removal of the quartz window. Through the first  $\sim 3000$  s of the experiment, the window was in place and the RDX was exposed to the radiation that passing through the quartz and those neutral atoms that found their way below the window to the film. The sharp drop in the signal at  $\sim 3050$ s was due to an interruption in the plasma itself. After the plasma was restarted at  $\sim 3150$ s, the intensities of scattered light returned to their previous levels. At  $\sim 3300$ s, discontinuities are observed in each curve. At this point in the experiment, the RDX sample was removed from the vacuum chamber, the quartz window removed, and the sample was reinserted into the plasma chamber all with the plasma operating at +50V applied bias. Following the discontinuity due to changes in lighting, each of the curves displays a new constant slope that is thirteen times the slope under the quartz window. Considering that the erosion rate under the quartz is only one thirteenth the rate of erosion under electron bombardment at +50 volts, which is the same as the rate of erosion under zero applied bias in hydrogen plasma, it is possible to conclude that the role of light in the erosion process is insignificant.

## II.E. Model of the Ignition Process

The model of the erosion of RDX in a hydrogen rich plasma proposed herein finds its origin in both the fundamental physics of ion-surface interactions and the fundamental differences between the combustion of primary and secondary explosives. The first step in this model is the implantation of hydrogen ions into RDX solid. The inherently larger mean free path of electrons, compared to ions, results a depletion of electrons from the plasma. As the number

of ions exceeds the number of electrons, a negative bias develops in the plasma. Under the influence of this negative bias, ions are driven from the plasma into any surface in contact with it. Due to their lower ionization threshold, the dominant species in a hydrogen plasma will be atomic hydrogen ions, hence an RDX surface exposed to a hydrogen plasma will experience frequent impact by atomic hydrogen ions. Using the hydrogen ion density calculated for the plasma emerging from an ETC igniter,<sup>2</sup> a flux of  $8.3 \times 10^{23} \text{ H}^+ \text{ cm}^{-2} \text{ s}^{-1}$  would result at any exposed surface,<sup>8</sup> which corresponds to a flux of  $\sim 1 \text{ H}^+$  ion per surface RDX molecule per nanosecond. The depth that these ions will implant will depend strongly on the plasma bias. Ion implantation of deuterium in carbon<sup>9</sup> in the 100-1000 eV regime is a well-characterized phenomenon. A large fraction,  $\sim 90\%$ , of the energetic ions will backscatter from the surface while the remaining 10% will implant into the solid. At the low end of the energy range, 100 eV, the ions implant at an average depth of  $100 \pm 30 \text{ \AA}$ , or  $\sim 35 \pm 10$  layers below the surface.

Ab-initio calculations<sup>10</sup> show that following implantation, the  $\text{H}^+$  ions will be rapidly neutralized by simple charge transfer to the surrounding RDX molecules. Additional ab-initio calculations<sup>10</sup> indicate two mechanisms for the reaction of the neutral hydrogen atoms with the surrounding RDX molecules. In the first, the hydrogen atom (radical) is attacked by one of the

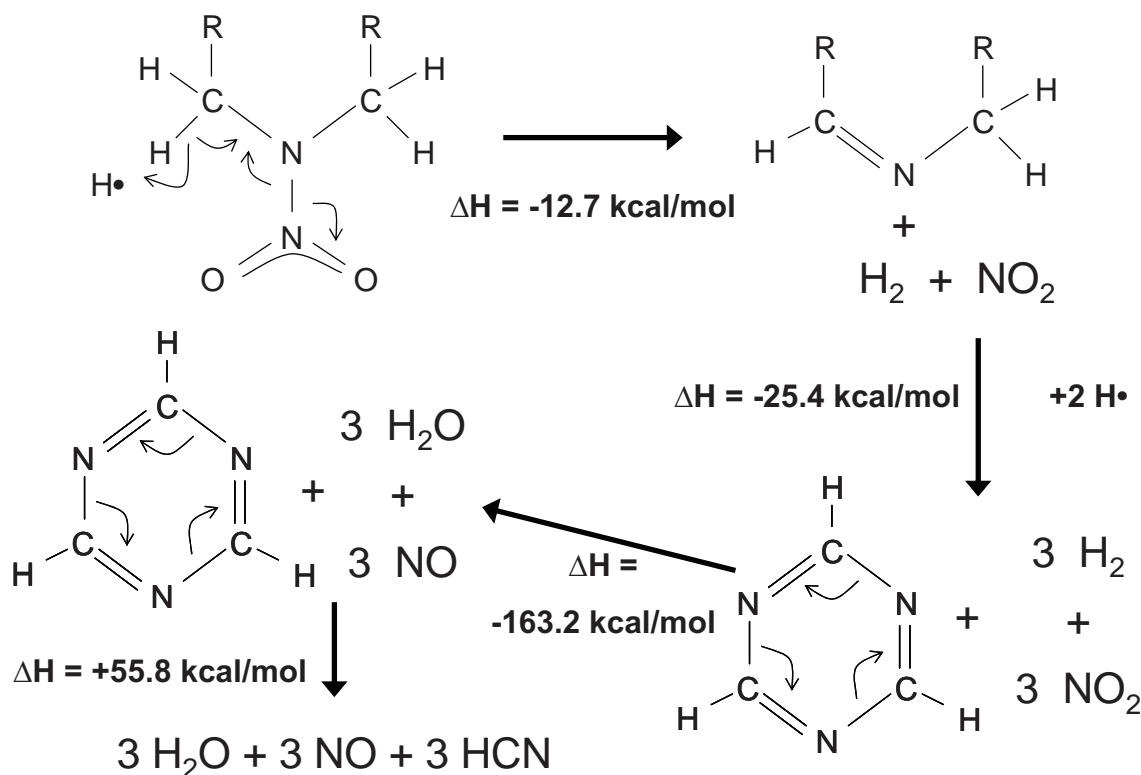


Figure 12 – The proposed mechanism of hydrogen atoms implanted in RDX.

$\text{NO}_2$  moieties of the RDX, resulting in the formation of a HONO molecule and leaving a radical at the ring nitrogen site where the  $\text{NO}_2$  used to be bound. This reaction, closely resembling the first step of the thermal decomposition mechanism known as the “HONO” mechanism, is found to be slightly endothermic at  $+0.6 \text{ kcal/mol}$ . Being endothermic and resulting in reactive species trapped below the surface in close proximity in the same cavity, the ultimate outcome of this

mechanism would most likely be only the recombination of the HONO and the RDX radical product. The second mechanism that was investigated was attack of the implanted hydrogen atom by one of the hydrogen atoms on a ring carbon, resulting in the formation of a hydrogen molecule and a radical on the carbon atom, resulting in the spontaneous release of a neighboring NO<sub>2</sub> group as a double bond forms between the ring carbon and the ring nitrogen. As opposed to the first mechanism, the first step of the second mechanism is exothermic at -12.7 kcal/mol. In addition, resulting in the formation of three stable products, the initial step of the second mechanism is not going to be highly reversible. The second step of this mechanism is the reaction of the initial products, H<sub>2</sub> and NO<sub>2</sub> to form NO and H<sub>2</sub>O, which is very exothermic, releasing an additional 54.4 kcal/mol into the reaction zone of ion implantation in the solid.

Under the high implantation rate described above, one might imagine the reaction of three implanted H atoms with the one RDX molecule, resulting in formation of 3 NO and 3 H<sub>2</sub>O and leaving 1,3,5-triazene. The 1,3,5-triazene might then decompose into 3 HCN molecules, producing a net of nine gas molecules in a cavity only the size of a single RDX molecule while at the same time releasing 145 kcal of heat, see figure 12. The resulting local pressure and temperature that would result for this process or even as the outcome of partial reaction would most certainly exceed the threshold for spontaneous combustion, resulting in the formation of a “hot spot”. At the implantation rates of one ion per nanosecond per molecular site a sufficient density of hot spots will be created, ultimately merging into a detonation front in a matter of only a few nanoseconds, consistent with the fast and reproducible ignition observed in ETC.

## II.F. A New Understanding of RDX Insensitivity, Ignition, Combustion and Detonation.

Another way to understand the proposed ignition mechanism is to view the implantation of H<sup>+</sup> as the route to a new chemical mechanism that alters the physical and chemical mechanism of ignition from that of an insensitive secondary explosive to one that more closely resembles that of a sensitive primary explosive. To clarify, one must consider what distinguishes a fast chemical reaction from an explosion. In a fast chemical reaction, the early acceleration in the reaction rate slows to a maximum as either the influx of reactants becomes limited or as a local heat balance is achieved. In an explosion, the rate of reaction escalates out of control due to branching radical reactions and/or thermal run-away. When considering homogenous condensed-phase materials, the supply of reactant is always high, hence the flux of reactant will rarely be the limiting factor. That leaves thermal run-away as the prime distinguisher between fast reaction rates and explosions. In terms of thermal run-away, reactions which release the most heat the most rapidly would be the most sensitive. Consequently, the materials that are the most sensitive, typically primary explosives, would be those in which the first reaction step is highly exothermic, and the least sensitive explosives would be those where the first step is endothermic, typically secondary explosives like RDX.

The key to the intrinsic insensitivity of RDX is the fact that the initial step, production of the initial gas products that fuel the flame is endothermic by 23 kcal/mol. This means that in the absence of an external source of energy, such as the radiation arising from the flame in sustained combustion, the initial step would have the net effect of cooling the surface region. As the reaction proceeds, the surface region becomes progressively cooler, slowing the rate of subsequent reactions until the reaction ultimately ceases. In other words, without sufficient heat

from the flame, the first step is self-quenching. The inescapable consequence is that any stimulus which produces insufficient initial gas products to feed and/or sustain the flame or which fails to ignite the flame *will not ignite the RDX*. Therein lies the root of the inherent insensitivity of RDX.

The fundamental understanding that may be gained from this perspective is that the difference between failing to sustain a flame or accelerating it from deflagration to detonation is primarily dependent on the coupling of the energy from the flame to the endothermic surface reaction which in turn feeds the flame. Many of the macroscopic properties of the ignition of RDX can be understood as a simple direct consequence of the extent of damping of the feedback between the flame and the release of its fuel. From this perspective, the role of pressure in the threshold for ignition can be found in how ambient pressure affects the coupling of energy from the flame to the surface. As the ambient pressure is increased, the initial gas products released from the surface will undergo a greater number of collisions per distance traveled. In traditional gas phase kinetics, each collision has the same probability of reaction, thus, an increase in the collision rate will result in a more rapid initiation of the reaction of the initial gas products. Since the initial gas products flow away from the surface, earlier initiation means the flame will form closer to the surface. From the perspective of fluid dynamics, increased ambient pressure means greater resistance to the expansion of the initial product gas flows from the surface, impeding its penetration into the ambient and compressing the flame nearer the surface. A closer flame means a better energy coupling between the flame and the surface, allowing the acceleration of the ignition process toward detonation even with a smaller initial stimulus. Lower ambient pressure will have the reverse effect, a decrease in the collision frequency or more efficient forced flow of the initial products. Either way, reducing the ambient pressure will result in a flame that is farther from the surface, reducing the coupling and making extinction of the flame more likely.

The existence of a critical diameter for detonation is another ignition phenomenon that is readily explained in terms of this model. In samples with diameters less than the distance to the flame, the diffusion, or forced flow of the initial gas products, will be spherical. In spherical transport, the initial gas products become diluted with ambient air. Diluted fuel results in a cooler flame and makes extinction of the flame more likely. Hence, samples with diameters significantly smaller than the surface to flame distance will not detonate. In samples that are larger than the surface to flame distance have linear diffusion, or linear forced flow. In either case, no dilution of the initial gas products occur as they are transported to the flame. With its fuel arriving at its maximum concentrations, the flame will obtain its maximum temperature and will have its greatest potential for accelerating the rate of reaction to the point of detonation.

### III. Laser Ignition of RDX Using Polymer Overlayers

If RDX can be ignited by the atomic plasma formed by the capacitive ablation of a polymer tube in ETC, would it be possible to ignite RDX with the atomic plasma formed laser ablation? This is the question that has motivated our research into the laser ablation of polymers, RDX and thin films. Our efforts can be divided into two distinct branches: experiments designed to obtain evidence of ignition (or failure to ignite) and experiments

designed to probe the fundamental processes involved in the laser ablation of polymer films, glass and RDX.

### III.A. Gas Pressure Jump Studies.

Our first efforts to determine if RDX could be ignited through ablation of a polymer overlayer were previously described in the Masters Thesis of Artem Dyachenko.<sup>5</sup> Briefly, a sealed volume chamber was constructed of four-way cross (0.75" I.D, 3.00" total length). A quartz window was mounted on the port opposite a blank flange to which a ~2.75" long 0.5" O.D. aluminum standoff was attached. RDX spot samples,

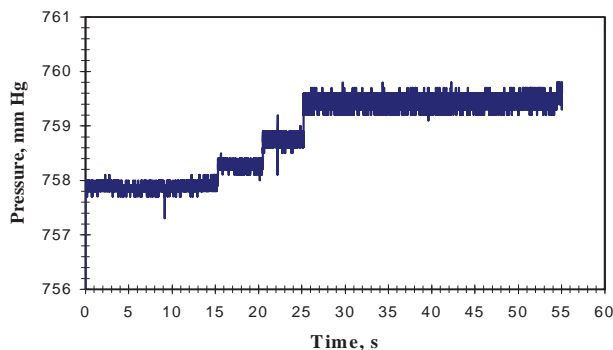


Figure 13 – Pressure trace of the ablation of bare RDX

deposited on pieces of glass slides as described in Section II.B., were mounted on the aluminum standoff with double sided tape. A Baratron capacitance manometer and a valve to vent and evacuate the chamber were mounted on the remaining two ports. Laser ablation of the polycarbonate, RDX and the polycarbonate coated RDX was achieved using a Continuum Inlite-III-10 Nd-YAG laser operating in the fourth harmonic mode at 266 nm with 5 ns pulse width. Laser fluence was maintained constant in all experiments by using the same laser setting, 190 ns Q-switch delay, 1300V on the flashlamps and constant laser focus of 100 mm using a 140 mm lens. The laser fluence selected was chosen such that a penetration of a 1.0 mg spot of RDX was achieved in three laser shots, as evidenced by the observation of a hole completely through the RDX spot, see figure 5. The pressure trace measured during the ablation of a bare RDX spot is shown in figure 13. Three distinct pressure jumps of ~0.5 mm Hg were observed to occur at times corresponding to the laser frequency of 0.2 Hz used in the experiment. This data is taken as direct evidence that each laser shot converts only a specific volume of RDX into gas. The fact that the second and third laser shots are focused at the same location on the RDX spot and still generate gas indicates that laser ablation of RDX does not trigger ignition of the RDX. Had ignition occurred, the combustion following ignition would have converted all of the material below the first laser shot to gas leaving no material to be converted to gas by the second and third laser shots.

To explore the possibility of RDX ignition by a polymer plasma, 1.0 mg RDX spots were spin-coated with polycarbonate. The depth of the ablation pit formed by each laser shot at the same 100 mm focus used in the bare RDX experiment was determined to be 0.6  $\mu\text{m}$  using commercial 254  $\mu\text{m}$  thick films by recording the number of laser shots necessary to result in complete penetration of the film, i.e. resulting in the formation of a hole. In the early pressure measurement experiments, the polycarbonate overlayers were typically 30  $\mu\text{m}$  thick, meaning that approximately 50 laser shots would be required to penetrate the bulk of the polymer film before the interface is exposed and the final polycarbonate ablation plasma is formed at the surface of the RDX at the interface. Pressure measurements made during laser ablation of pure

polycarbonate films revealed no net pressure increase upon ablation. To explain this observation one must consider that the complete combustion of one polycarbonate repeat unit ( $C_{16}H_{14}O_3$  (s)) to  $CO_{2(g)}$  and  $H_2O_{(l)}$  consumes two more gas molecules than it produces, while incomplete combustion to  $CO_{(g)}$  and  $H_2O_{(l)}$

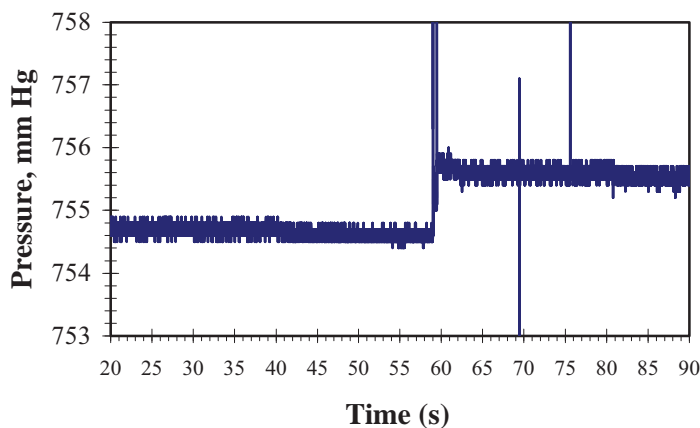


Figure 14 – Pressure trace of the ablation of polycarbonate coated RDX

produces six more gas molecules than it consumes. Hence, the observation of no net pressure effect simply implies combustion that results in roughly three times the number of  $CO_2$  molecules than  $CO$  molecules. Pressure measurements made during the laser ablation of a polycarbonate coated RDX film at a laser frequency of 0.2 Hz is shown in figure 14. Upon the 43<sup>rd</sup> laser shot, at ~60s into the data collection, a single pressure jump of ~1.4 mm Hg is observed. This single pressure jump has a magnitude that is equivalent to that of the three pressure jumps and is observed to occur as the result of just one laser pulse and no subsequent pressure jumps are observed. The most reasonable conclusion is that the 43<sup>rd</sup> laser pulse ignited the underlying RDX converting it all into gas. Unfortunately, there was no obvious way to prove that the laser shot that ignited the RDX was impinging on the last remaining layer of polycarbonate, so alternative methods of confirming the ignition of RDX were initiated.

### III.B. Photographic Image Studies

The process of the laser ablation involves the rapid formation of gas/plasma and the subsequent expansion of that gas/plasma plume into the ambient. Expansion into the ambient may result in reaction of that gas/plasma with the ambient. For instance, a mushroom shaped fireball is observed as the result of the ablation of a polycarbonate film, see figure 15. Although measurable plumes were observed for the ablation of glass and RDX, no fireballs were



Figure 15 – Fireball created by the ablation of polycarbonate in air.

observed for these materials. This led to the conclusion that the optical image of the plume depends not only on the volume of gas generated but also on the chemical nature of the products formed. And, the chemical nature of the products will depend not only on the material ablated but also on the chemical processes taking place. This led us to begin optical studies to distinguish between the ablation of RDX and ignition of RDX, through the comparison of images taken from bare and polycarbonate coated RDX.

The fundamental assumption of this approach was that the size, color and intensity of optical emission from the plumes of different materials of the same material undergoing a different chemical mechanism might be readily distinguished from photographic images obtained of the plumes. To recognize the difference between the ablation of RDX or ignition of RDX following ablation of the polycarbonate overlayer requires the individual characterization of the ablation of polycarbonate, bare RDX and the glass slide onto which the RDX was deposited. Since the glass did not ablate under our laser conditions, we did not need to be concerned with it.

Lacking a way to synchronize the acquisition of photographic images with the pulsing of the laser, the only way to acquire images of the short lived plumes was using continuous acquisition in the video mode of the camera. Since the ablation of RDX does not result in the formation of a bright fireball, all videos for analysis were obtained in the dark so that the RDX plumes could be imaged and directly compared to the polycarbonate images. Operating the laser at 1Hz, videos obtained at a rate of 15 frames per second yielded single frame images of the plume every 15<sup>th</sup> frame. All of the other 14 images were completely blank. We occasionally observed a single frame shift of the frames containing images of the plume, but tests on polycarbonate yielded image frames with a constant intensity, leading us to conclude that the video mode simply integrated the light for nearly the full 1/15 of second. The downside of the video mode is video frame image resolution. In picture mode, the Pentax Optio S5i camera that we use collects 2560 by 1920 pixel images, while in the video mode it only collects 640 x 480 pixel video frames. As a result, the resolution of the video frame images taken of the plumes are not as sharp as the photographic image of the polycarbonate plume taken at 10 Hz laser repetition rate in figure 15.

Video images obtained while ablating bare RDX at a laser frequency of 10 Hz are shown in figure 16. All of the images were obtained with the

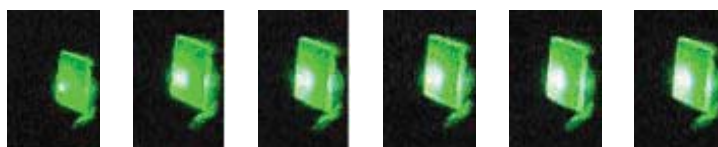


Figure 16 – Successive video images obtained during the ablation of bare RDX.

camera  $\sim 60^\circ$  from the sample normal. Each image is the light collected from a  $\frac{1}{2}$ " by  $\frac{1}{2}$ " glass square cut from a glass slide onto which a standard RDX spot was deposited in the lower left corner. In addition to the light coming directly from the surface of the substrate, each image includes a crescent to the lower right of the substrate and a bright spot to the center right of the substrate. The crescent is simply a reflection of light from the surface by clip that holds the substrate in place. The bright spot on the left is believed to be light which was channeled into the substrate only to finally escape through the edge of the substrate.

The first thing that might be noticed in the sequence of video images is that no plume is observed. As mentioned above, plumes were only optically observed arising from polycarbonate ablation where the gas/plasma products are presumed to combust at the contact surface where they mix with ambient air. The next thing one might notice is that the white region in the lower left corner of the sample grows in each of the first three frames and then remains constant in all subsequent frames. Considering that the RDX spot and laser settings used in these experiments were identical to those used in the pressure jump experiments (Section III.A.), it is not surprising that it takes three laser shots to reach the final state of the images, if that final state is assumed to represent the formation of a hole entirely through the RDX film.

What is more interesting is that first two images show progressively larger white spots. If the first two laser shots simply thinned the RDX spot in the region of illumination, one would think that the reflective properties of the spot would remain the same. However, this is not what is observed. Instead, the white region grows in each of the first three images as does the white spot to the center right of the substrate. One possible explanation of this phenomenon might be found in the roughness of the RDX spot. It is well-established that the RDX spot is composed of individual crystallites. It is not completely unreasonable to think that in certain small regions the RDX spot may only be as thick as the depth of the ablation pit formed by a single laser shot. Hence, very small regions of the film may be penetrated with the first laser shot. These “micro” holes might then be the channels by which light may enter the glass slide during the first two laser shots.

Video images obtained while ablating polycarbonate coated RDX at a laser frequency of 10 Hz are shown in figure 17. All of the images were obtained under conditions identical to

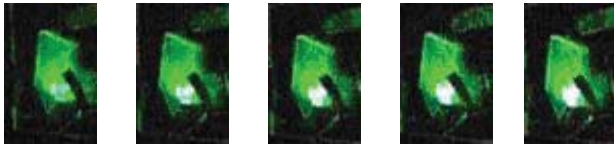


Figure 17 – Video images obtained during the ablation of polycarbonate coated RDX

those used in the experiments on bare RDX. The only significant difference between the polycarbonate coated RDX spots used in these experiments and those used in the pressure jump experiments is the thickness of the polycarbonate films used. Prior to these experiments, we

refined our spin-coating technique to allow the deposition of polycarbonate layers of less than a micron thickness, allowing us to ablate them in a single laser shot. All of the images show a multi-lobe bright region in the lower right corner of the glass rectangle. The most striking feature of the figure 17 is that after the first image, all of the images are virtually indistinguishable, leading to the logical conclusion that the process reaches its final state in just one laser shot. A more detailed analysis of the images reveals that the top two are the both the largest and least variable in the images. We believe this to indicate that they are the direct image of the laser irradiated spot and the light channeled through the glass substrate and then out the side. The lower two lobes are smaller in all of the images and are much dimmer in the first image. We believe the left lower lobe to be light channeled through the glass substrate that escapes out the bottom edge of the glass substrate and right lower lobe to be an internal reflection from the bottom edge that escapes out the side edge of the glass substrate. We believe that the reduced intensity of all lobes reflects the fact that the bulk of the RDX film was not removed from the laser irradiated area until the end of the first laser pulse. Assuming a normal detonation velocity of 8440 m/s for RDX,<sup>11</sup> ignition of the 30  $\mu\text{m}$  thick RDX film should take 5 ns which is roughly the pulse duration of the laser. It should lastly be noted that such a clear observation of ignition through photographic documentation has not proved to be highly reproducible. Among the many experiments with polycarbonate coated RDX, a minority showed removal of the film only after several laser shots. Although we believe that this was the result of incomplete polymer coverage, we are currently unable to prove that hypothesis. To do so would require a technique capable of distinguishing the chemical nature of the exposed surface layer with resolution of at least 1  $\mu\text{m}$  and a total imaging area of at least 1 mm. We believe that an automated wide-scan scanning probe microscope<sup>12</sup> operated in friction or phase mode could easily distinguish exposed RDX from the polycarbonate coating.

### III.C. Outlook for Future Progress in Photographic Imaging

Overall, our efforts to photographically document the ignition of RDX using photographic methods have proved inconclusive. They are, however, continuing through the use of the image details previously ignored, such as the red to blue ratio, which preliminary investigations have indicated can be used to distinguish between polycarbonate and RDX plumes. In addition, the laser ablation apparatus has been modified by the addition of a microscope, which has been modified for use of our camera, to allow greater resolution of the images of the plume. We believe that, using the microscope, we will be able to resolve the differences in the size of the plumes that arise from (1) laser ablation of polycarbonate which converts  $0.6 \mu\text{m}$  of solid to gas per laser shot, (2) laser ablation of RDX which converts  $6 \mu\text{m}$  of solid to gas per laser shot and (3) ignition of the RDX spot which converts  $30 \mu\text{m}$  of solid to gas in a single laser shot.

### IV. Fundamental Studies of Laser Ablation

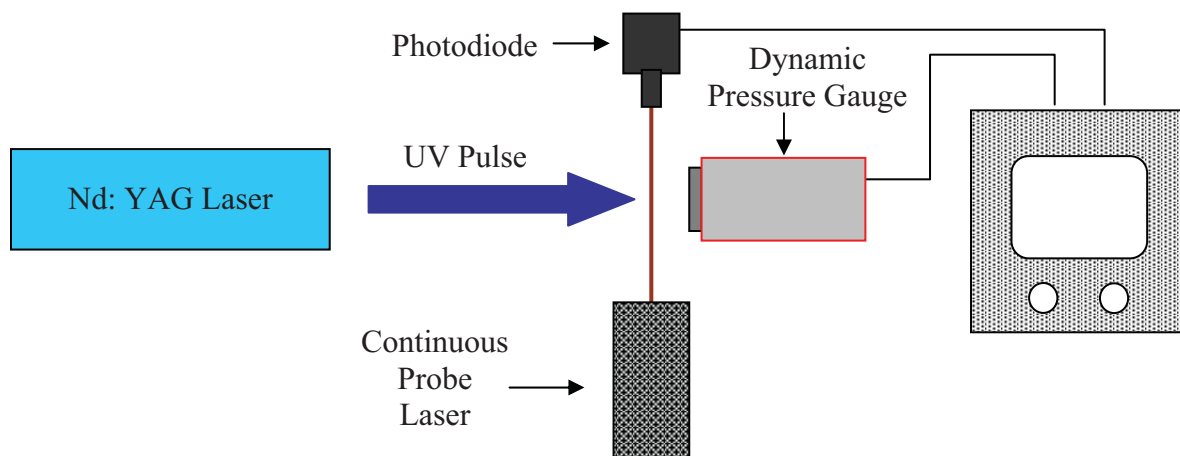


Figure 18 – Experimental apparatus used in dynamic pressure measurement and photodeflection experiments

#### IV.A. Dynamic Pressure Measurements During Laser Ablation

The dynamic pressure measurements described below were begun to detect direct evidence of the ignition in polycarbonate coated RDX films. The apparatus used is shown in Figure 18. After the acquisition of many data sets, it became apparent that these experiments were far too complex to allow such simple interpretations. After failing to reach any significant conclusions, this line of investigation was ultimately abandoned to devote more effort to the photodeflection studies (Section IV.B. and IV.C.) that had proved far more informative. As these investigations were concluded in the third year, but have yet to be published in the open literature, the description of the dynamic pressure experiments previously included in our interim progress reports is re-presented below for completeness of this report.

The first dynamic pressure measurements were laser ablation of 254- $\mu\text{m}$  thick industrial polycarbonate films. In these and all laser ablation experiments, the pressure gauge is driven into oscillations, which resemble those of a single oscillator system. Upon recognizing that the frequency of oscillations for a single oscillator can be used to determine the mass of the oscillator, investigations were begun to use the frequency of the oscillations to determine mass loss upon ablation. Fourier analysis of the pressure versus time signals obtained with different masses of industrial polycarbonate (masses ranging from 0.0025g to 0.0065g.) attached to the gauge by scotch tape or glue revealed that not only did the frequencies shift, but multiple new peaks appeared. That result was interpreted as meaning that the device is not actually a single oscillator system, but a system of coupled oscillators that are engineered to produce a single frequency response. Based on this hypothesis, it still seemed possible the mass loss upon ablation could be measured, if the mass added to the gauge were small. To this end, an RDX spot of mass  $0.0002 \pm 0.0001\text{g}$  was sprayed directly onto the gauge. Unfortunately, new frequencies still appeared in the Fourier transform and the line of investigation was terminated. To avoid disrupting the apparently fragile, engineered balance of the pressure gauge, a new sample geometry was adopted, see figure 18, in which no additional masses are directly attached to the pressure gauge.

Preliminary measurements of the general characteristics of dynamic pressure measurements were carried out on free standing polycarbonate films that were installed in front of dynamic pressure gauge. The rest of the experimental set-up used in the first measurements is shown in figure 19. Laser ablation was accomplished using the fourth harmonic of a Continuum Inlite Nd:YAG laser, producing a 6ns pulse of 45 mJ at 266 nm. The miniature dynamic pressure gauge was a PCB 113B37,

specifically designed for shock tube and blast wave measurements with a maximum pressure of 6895 kPa, a resonant frequency more than 400 kHz and rise time less than  $1.5\mu\text{s}$ . The output was amplified with a PCB 482A22 signal conditioner and the output signal was recorded with a Tektronix TDS1001B 40MHz digital oscilloscope. The signal from a Ultrafast Sensors FCX033 photodiode (sensitivity, 350-1100 nm and active area  $125\mu\text{m}^2$  in diameter) was

installed in front of IR channel and connected to a PS-5 amplifier, was recorded in second channel of oscilloscope and used as the trigger for the oscilloscope. The time delay between Q-switch signal of the laser and initial rise of laser pulse of IR channel was measured to be  $0.26 \pm 0.02\mu\text{s}$ , and the delay between laser pulse and peaks of PG signals was  $0.72 \pm 0.04\mu\text{s}$  for both samples investigated. Pressure measurements on sandwich structures of

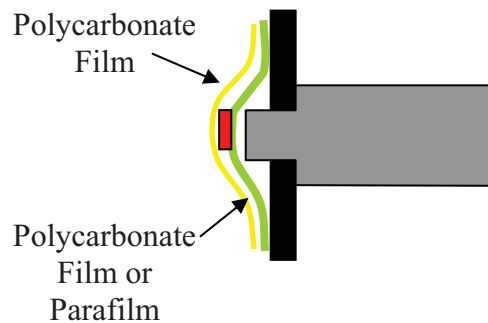


Figure 19 – Sandwich structure used to reduce mass addition to the pressure gauge

polycarbonate/RDX/polycarbonate (left) and polycarbonate/RDX/parafilm (right) are presented in figure 20, with the first laser shot on top and successive laser shots appearing below. Based

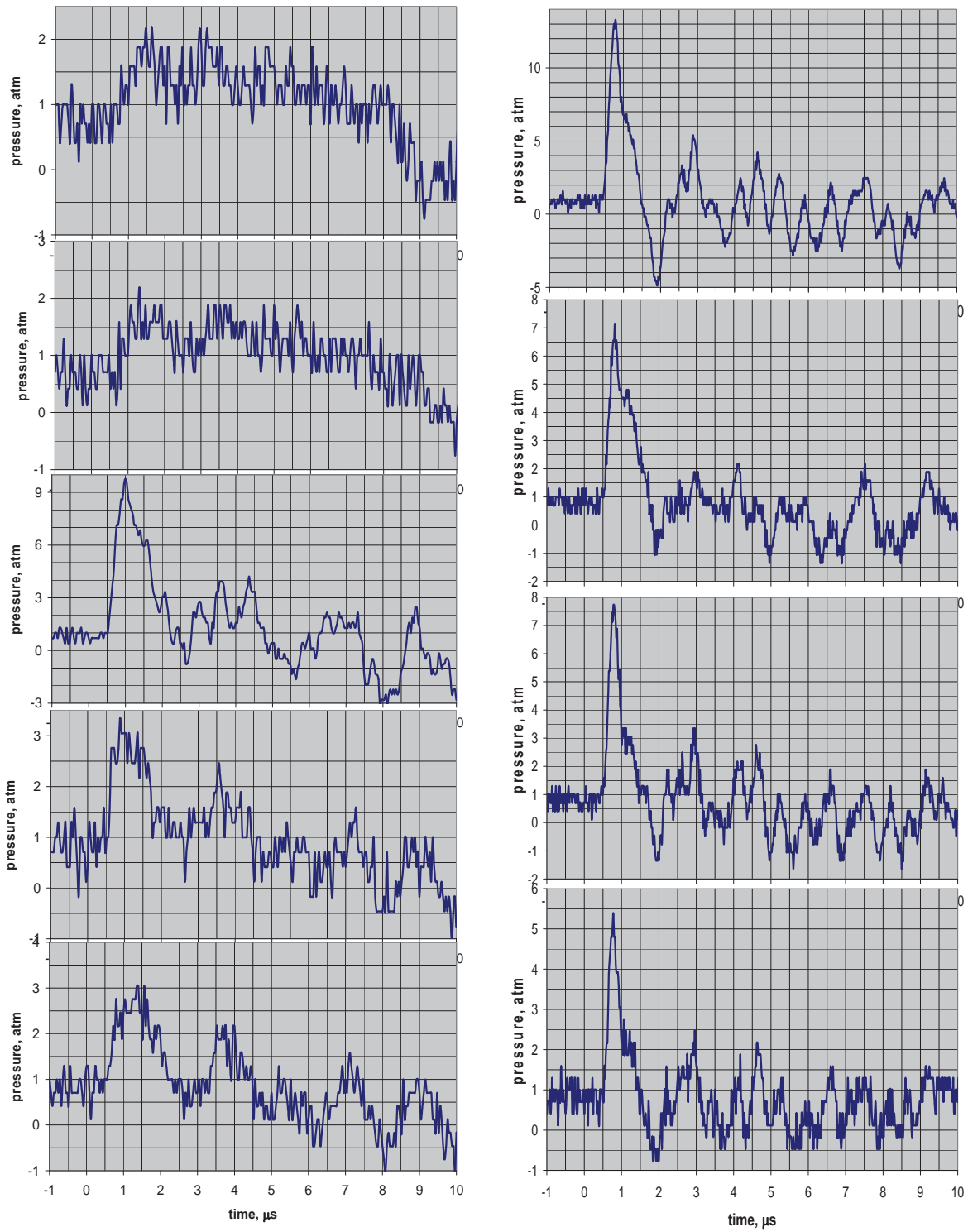


Figure 20 – Dynamic pressure measurements of sandwich structures of polycarbonate/RDX/polycarbonate (left) and polycarbonate/RDX/parafilm (right)

on the static pressure calibration curve, pressure peaks up of 10 atm and 15 atm, are observed for the two structures, respectively. For the polycarbonate sandwich, first two measurements are believed to correspond to the ablation of only the top polycarbonate, while the latter three measurements are believed to be combinations of RDX and polycarbonate. For the polycarbonate/RDX/parafilm structure, the oscillations observed in the latter three plots on the left are not observed. This is believed to be due to damping caused by contact of the parafilm with the working surface of dynamic pressure gauge. For both sets of experiments, where the ablation of RDX is believed to contribute to the pressure, a shoulder appears on the downward slope of the initial pressure rise. This shoulder would not be predicted for either the expansion of a fixed volume of gas or the propagation of the shockwave across the pressure gauge. The observation of this shoulder implies a sudden jump in either temperature or the amount of gas present. At this point, we cannot identify the exact source of the shoulder, but take it as possible indication of detonation of the RDX below the material ablated.

Finally, a comment needs to be made as to how a model of the process that includes detonation of the RDX below the ablation event can be compatible with the observation of multiple laser shots with similar pressure profiles. If the polycarbonate and RDX layers were perfectly smooth, then the entire surface of the each material would be expected to be contacted by the ablation event at the same time. However, if the polycarbonate and/or RDX film are rough, with respect to the ablation depth (typically 0.6  $\mu\text{m}$  for polycarbonate), then over some regions of polycarbonate surface the ablation event might reach the interface and trigger detonation, while over other regions of the surface a polycarbonate layer may remain over the interface, delaying detonation until a subsequent laser shot. The magnitude of the roughness can be best understood by considering that the 16 $\mu\text{m}$  RDX film is composed of primarily 10 $\mu\text{m}$  crystals.

#### IV.B. Laser Ablation of Polycarbonate and Glass

The results presented in this section have been recently published in the Journal of Applied Physics in 2009.<sup>13</sup> Since the published account contains a complete account of our current understanding, only a brief review of the salient conclusions will be included herein.

Photodeflection was measured following laser ablation of polycarbonate and glass surfaces using the apparatus shown in figure 16. Ablation was achieved through irradiation of the surfaces using the same Continuum III-10 Nd:YAG laser operating in the fourth harmonic mode described in previous sections. Photodeflection signals were generated as the index of refraction of the gas between probe laser (Larsaris DSLC continuous beam diode) and the detector (Ultrafast Sensors FCX033 photodiode) changed following the laser ablation event.

Figure 21 is a plot of the photodeflection data obtained upon ablation of 1.0 mil polycarbonate films obtained from McMaster-Carr at a number of sample to detector/probe distances. The arrows indicate the evolution of the observed four features. The first feature (I) is the least well understood. Its velocity is too fast for any gas process, and consequently, is attributed to an electron pulse propagating through the residual plasma resulting from the

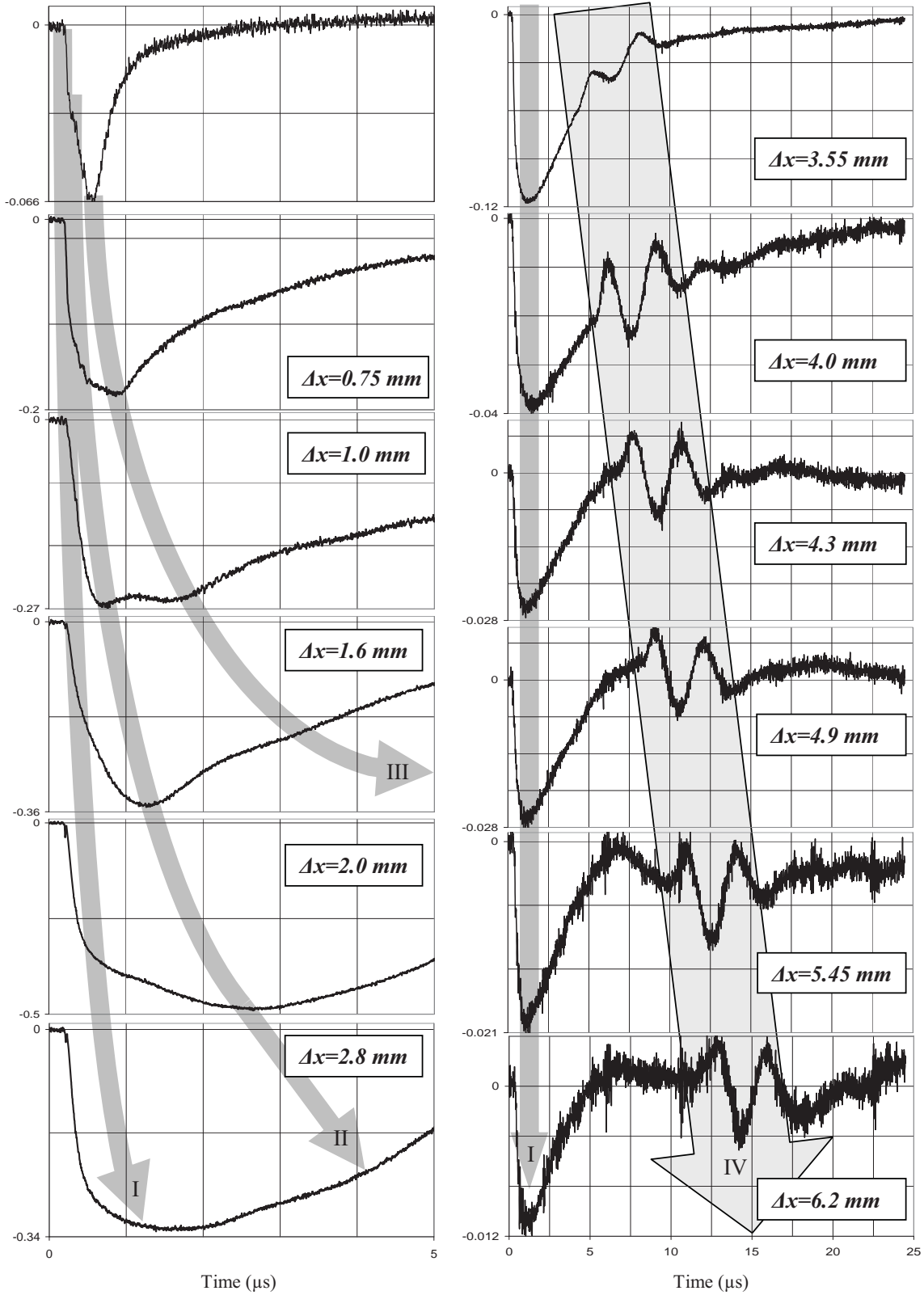


Figure 21 – Photodeflection curves for the ablation of polycarbonate as a function of surface to probe distance

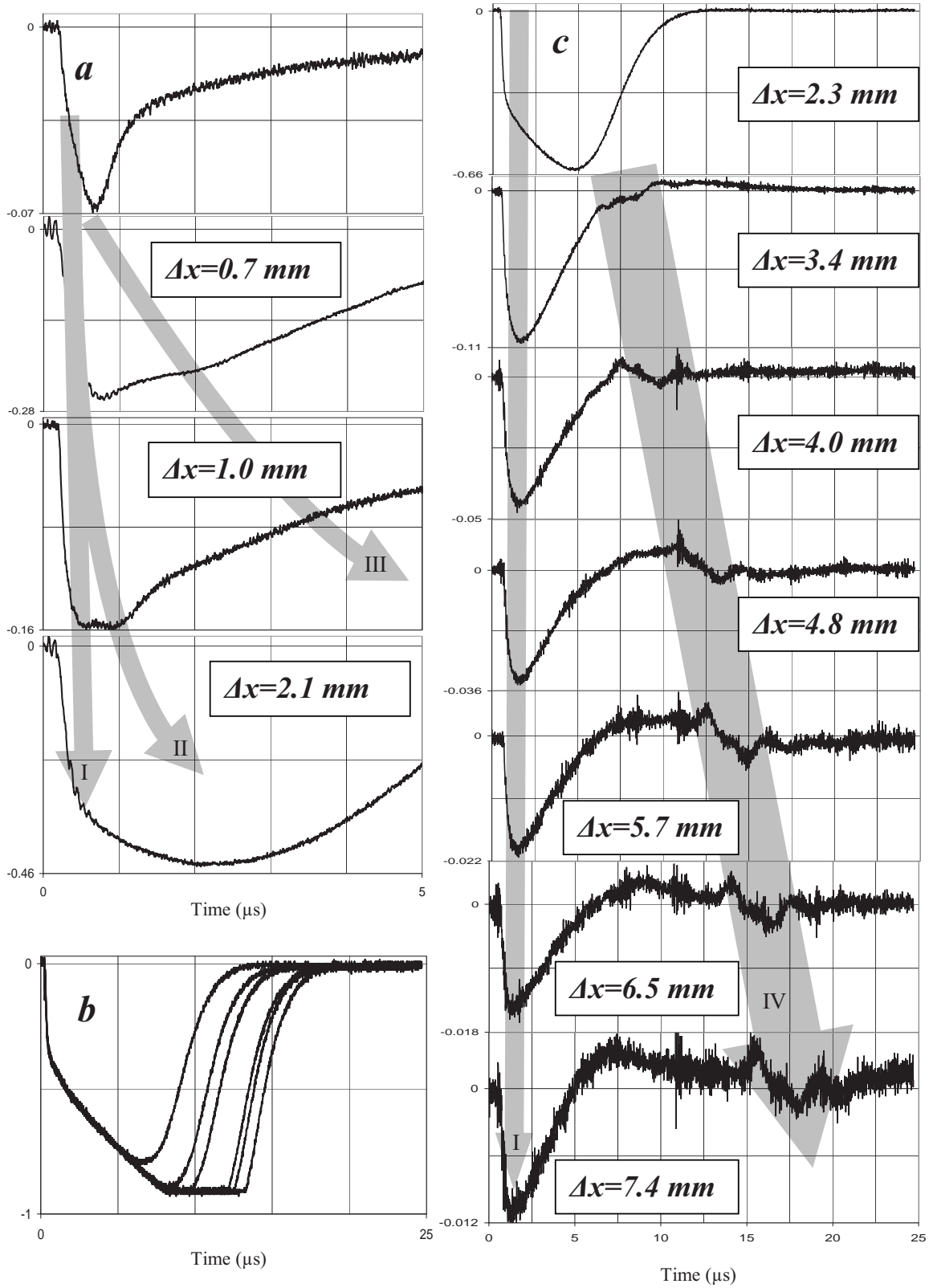


Figure 22 – Photodeflection curves for the ablation of glass as a function of surface to probe distance.

passage of the ablation laser. The second (II) and third (III) features are observed to sharply decelerate as they expand from the surface in ways that are consistent with their assignments as the shock wave and the ablation plume, respectively. The fourth feature (IV) moves at constant velocity and is assigned as originating in the popping sound heard whenever a surface is ablated. Figure 22 is a plot of the photodeflection data obtained upon ablation of borosilicate glass films obtained as Corning No.1 cover slips at a number of sample to detector/probe distances. Each of the features observed in the ablation of polycarbonate is observed in the ablation of the borosilicate glass. The only significant difference is that complete blocking of the probe laser is observed at 2.1 mm sample to detector/probe distance, see Figure 20b. In contrast to all other sample to detector/probe distances, the photodeflection curves at 2.1 mm are not indistinguishable when the experiment is repeated. Complete blocking of the probe laser is attributed to complete scattering of the probe laser light by  $\text{SiO}_2$  particles that condense as the ablation plasma cools. As evidenced by the narrow region of space in which complete blocking was observed, it appears that the formation of clusters occurs only in a very small volume of space.

#### IV.C. Photodeflection Studies of the Laser Ablation of RDX

Photodeflection studies were carried out on during the laser ablation of RDX. The principle difference between the experiments carried out on glass and polycarbonate and those carried out on RDX is that multiple shots on the same spot on glass and polycarbonate substrates yield reproducible photodeflection curves, while successive laser shots on the RDX produced noticeably different results. The data as a function of laser shot number and probe laser distance from the surface are shown in figures 23-28. The data clearly displays a elements that are consistent with those observed for the laser ablation of glass and polycarbonate, but a thorough interpretation has yet to developed. The data will be published after a complete interpretation of it has been achieved.

#### IV.D. Summary and Outlook for Future Progress in Photodeflection Studies

The results of the photodeflection studies on glass and polycarbonate have established a solid foundation for understanding the data already obtained on RDX. Among the achievements of those experiments was the observation of features corresponding to the gas dynamical phenomena know as the shock wave and the contact surface, the ablation plume itself. Also observed were the emanation of sound from the ablation event and a fast feature tentatively identified as electron ejection. Differences between the data obtained from the laser ablation of RDX and the previously studied non-energetic materials may reveal some new insight into how an energetic material behave as it is laser ablated. However, the strong similarities in shape between most of the photodeflection curves for RDX and those of the non-energetic materials lead us to believe that no significantly different phenomena will be discovered in the analysis of the RDX data. Consequently, at this point, we believe that unless the analysis of the RDX laser ablation data reveals something that we do not presently anticipate, further photodeflection studies will not be justified, as our efforts will be better spent pursuing the photographic evidence of ignition.



Figure 23- Normalized photodeflection data for the first laser shot on an RDX film.

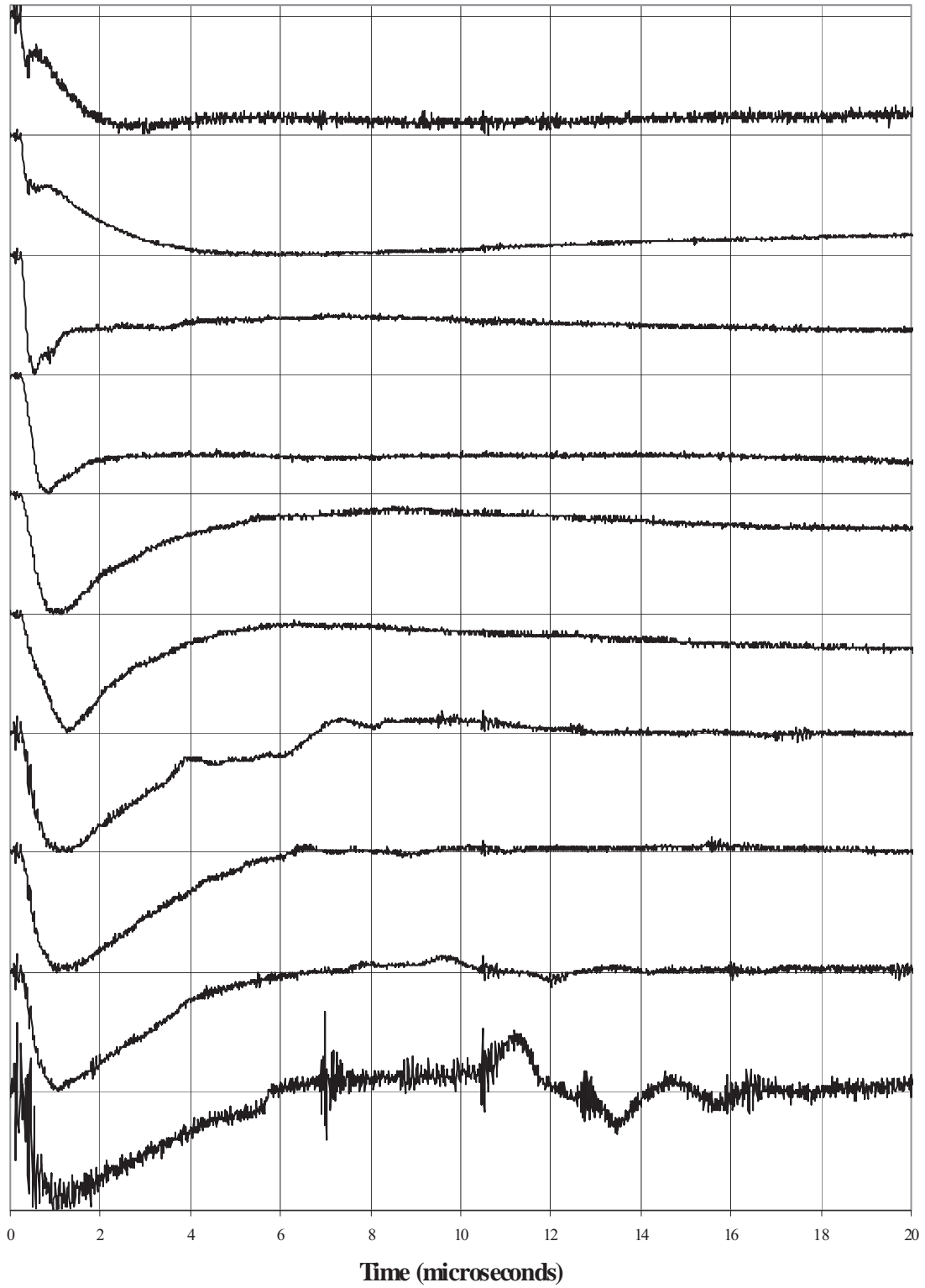


Figure 24 - Normalized photodeflection data for the second laser shot on an RDX film.

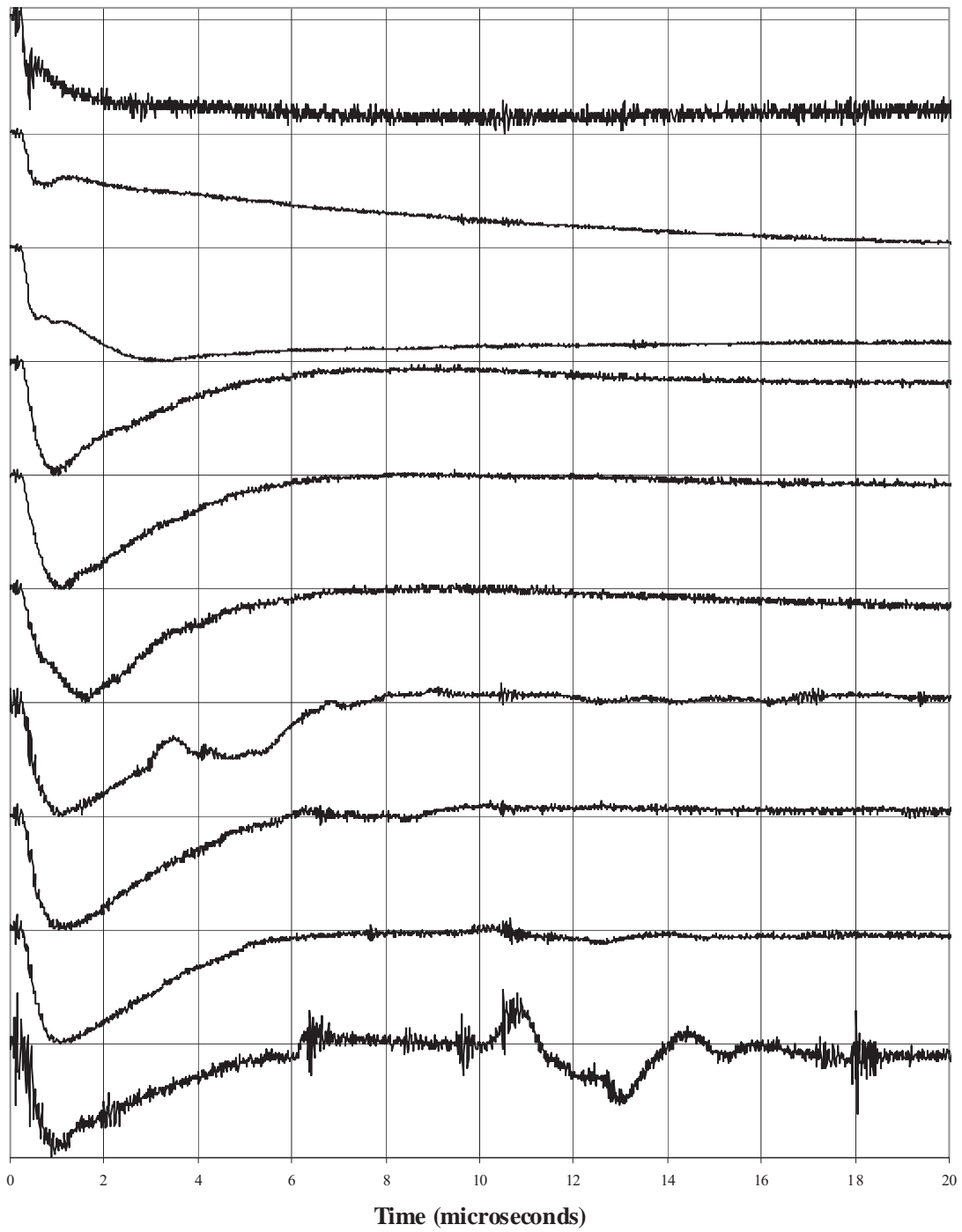


Figure 25- Normalized photodeflection data for the third laser shot on an RDX film.

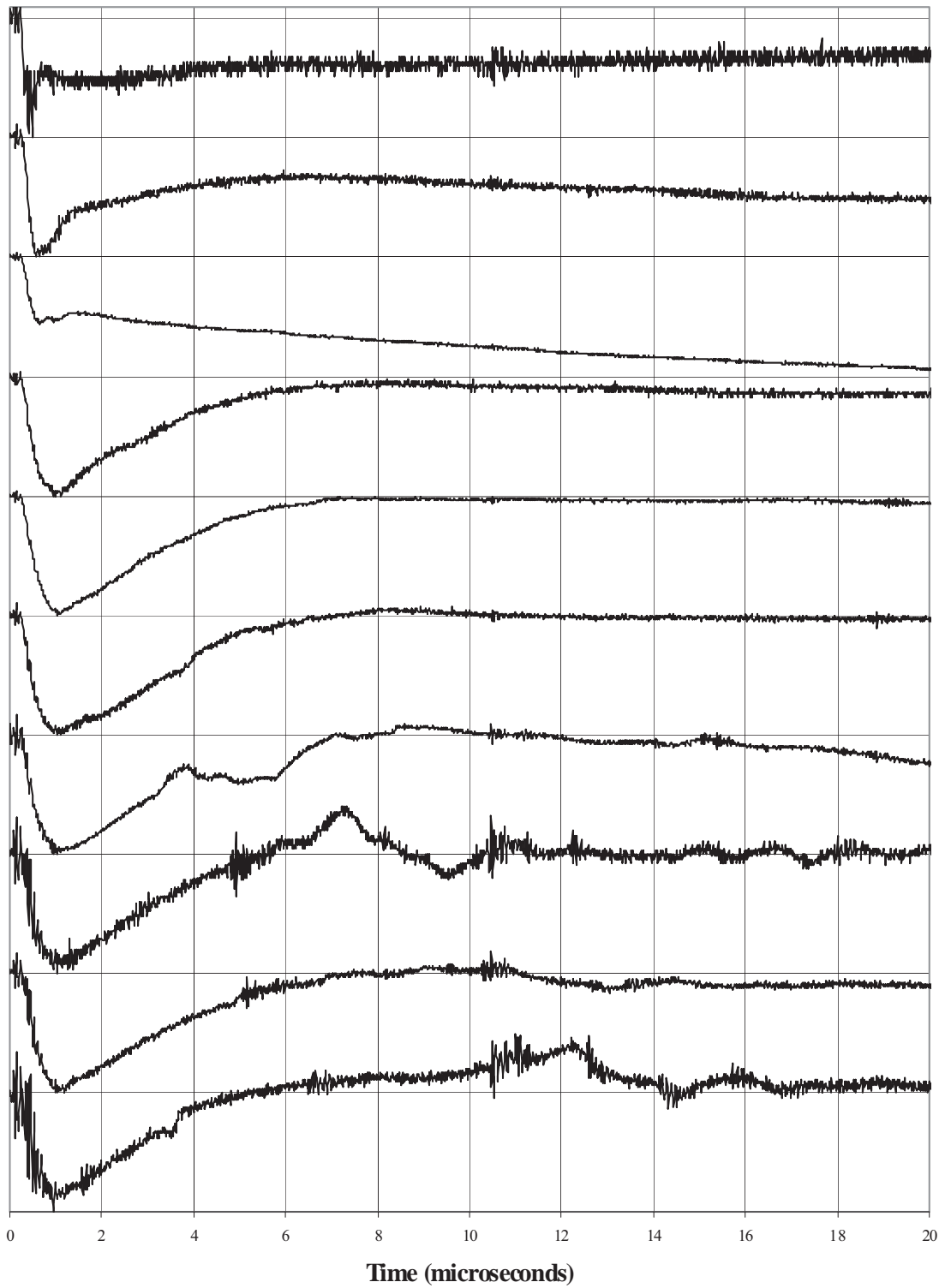


Figure 26- Normalized photodeflection data for the fourth laser shot on an RDX film.

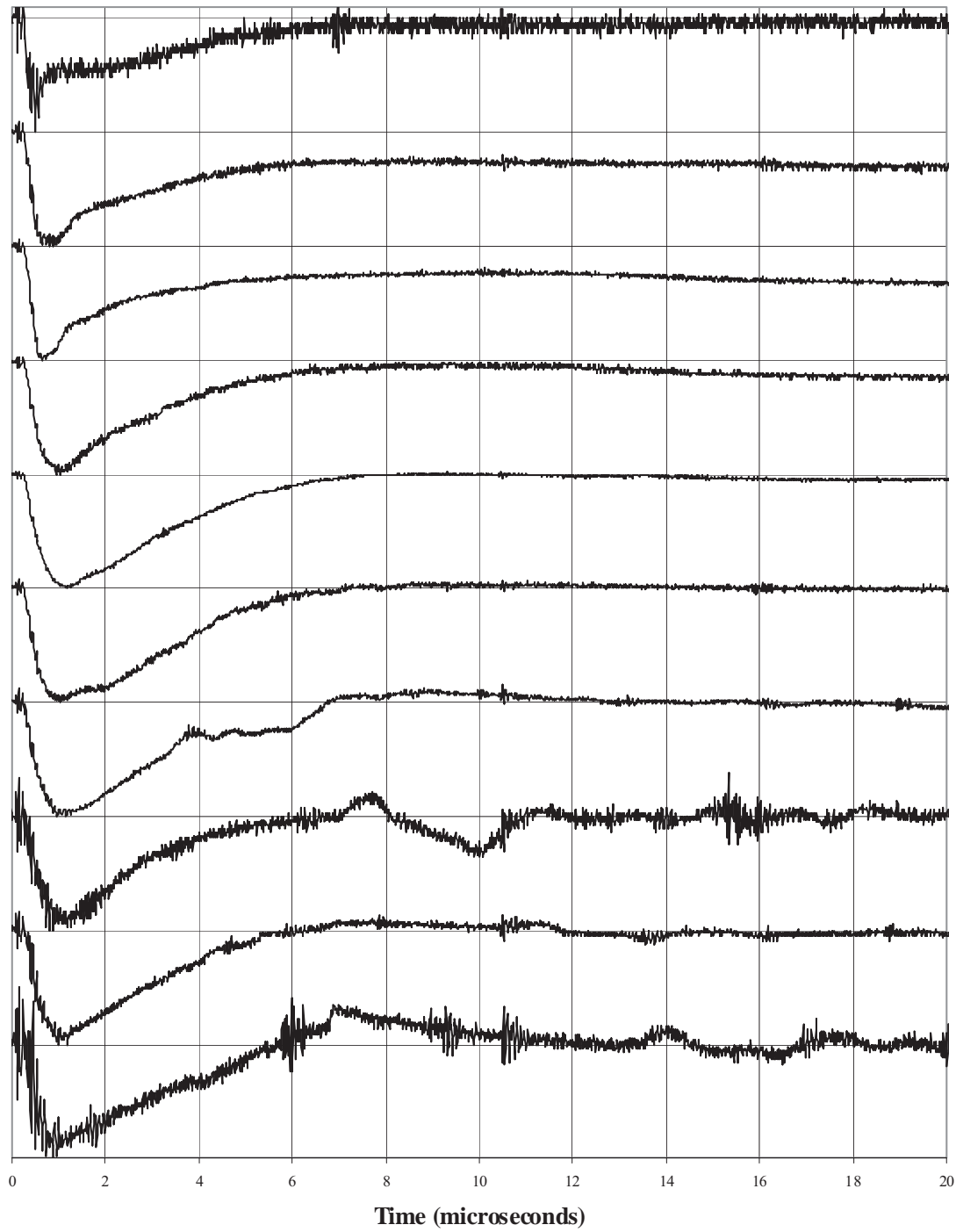


Figure 27 – Normalized photodeflection data for the fifth laser shot on an RDX film



Figure 28- Normalized photodeflection data for the sixth laser shot on an RDX film.

## V. Summary and Conclusions

Overall the research program, described herein, can only be described as a major success in that it has provided a substantive answers to two fundamental questions posed by ARO, “How does an ETC ignition work?” and “Why does ETC result in a short, reproducible ignition delays?” In addition, an alternative ignition method has been developed that preliminary results indicate is capable of igniting RDX with the same short, reproducible manner as ETC.

Our model of ETC ignition is based on the fact that virtually all plasmas, including the ones that emerge from the ETC igniters, develop a positive self-bias due to a higher rate of loss for electrons, resulting from their greater mean free paths. Exposed to a positively biased plasma, an RDX surface is subjected to positive ion bombardment, which in the case of hydrogen ions results in implantation roughly half of the time. Once implanted, the hydrogen ions neutralize before reacting with RDX to form  $H_2$  through the abstraction of hydrogen from the carbon atoms on the ring. Upon abstraction of a hydrogen atom from the ring, the carbon atom forms a double bond with an adjacent nitrogen, releasing a  $NO_2$  molecule. Trapped in close proximity below the solid surface, the  $H_2$  and  $NO_2$  react to form  $H_2O$  and  $NO_2$ , releasing a large amount of energy and creating a gas bubble of enormous pressure that drives the reaction of neighboring RDX molecules. Fundamentally, this reaction mechanism better resembles the reaction of a primary explosive, where the release of energy is coincident with the reaction front, as opposed to the normal combustion of RDX, where release of heat is isolated in the remote flame region.

The new method of ignition exploits the mechanism described above to ignite the RDX without the need for the large capacitors and power supplies that make ETC impractical. In this method, a plasma similar to the one that emerges from the ETC igniter is created at the surface of the RDX as the result of the laser ablation of a polymer film coating the RDX surface. Preliminary pressure jump and optical monitoring studies of the laser ablation of polymer coated RDX films have indicated that ignition does occur, but additional work remains necessary to unambiguously prove ignition. That work is continuing in our laboratory. Other methods originally begun as attempts to establish ignition, such as the dynamic pressure measurements and the photodeflection studies, have proved too complex to be used as proof of ignition, but instead became the foundation of an important understanding of the formation and evolution of the laser ablation plumes.

## Bibliography

- 1 J.W. Coburn and H.F. Winters, “*Ion- and electron-assisted gas-surface chemistry – An important effect in plasma etching*” **Journal of Applied Physics** 50(5) (1979) 3188-3196.
- 2 M.J. Nusca, M.J. McQuaid, and W.R. Anderson “*Numerical Model of the Plasma Jet Generated by an Electrothermal-Chemical Igniter*” **Journal of Thermophysics and Heat Transfer** 16(1) (2001) pp 157-160.
- 3 Rodney Valliere and Rik Blumenthal, “*Strong Synergistic effects in the combustion of propellants in H<sub>2</sub> plasmas*” **Journal of Applied Physics** 100 (2006) 084904.
- 4 A. Orland and R. Blumenthal, “*Nebulizing Spray Technique for Deposition of Propellant Thin Films*” **Journal of Propulsion and Power** 21(3) (2005) 571-3.
- 5 Artem Dyachenko, Studies on Laser Ablation of Polymer Coated Propellant Films, M.S. Thesis, Auburn University, August 7, 2006.
- 6 Z.L. Zhang, “*Comment on ‘Sputtering transport theory: The mean energy’*” **Physical Review B** 71 (2005) 026101.
- 7 Barbara J. Garrison and Zbigniew Postawa, “*Computational View of Surface Based Organic Mass Spectrometry*” **Mass Spectrometry Reviews** 27 (2008) 289– 315.
- 8 Daniel L. Flamm and G. Kenneth Herb, “*Plasma Etching Technology – An Overview*” in Plasma Etching – An Introduction, Dennis M. Manos and Daniel L. Flamm, eds. (Academic, San Diego, 1989) page 28.
- 9 D.M. Manos and H.F. Dylla, “*Diagnostics of Plasmas for Materials Processing*” in Plasma Etching – An Introduction, Dennis M. Manos and Daniel L. Flamm, eds. (Academic, San Diego, 1989) page 282-286.
- 10 M. McKee, Auburn University, Private communication.
- 11 J. Akhavan, The Chemistry of Explosives, 2<sup>nd</sup> Edition, RSC Paperbacks, (The Royal Society of Chemistry, Cambridge, UK, 2004) pp 58.
- 12 As described in DURIP Proposal 53734CHRIP: “*Topographic Imaging of Propellant Surfaces for the Investigation of Propellant Ignition*”
- 13 T.A. Bormotova and R. Blumenthal, “*Ultraviolet Laser Ablation of Polycarbonate and Glass in Air*,” **Journal of Applied Physics** 105 (2009) 034910/1-7.